

Spatial Characterization of Electromagnetic Random Channels

Andrea Pizzo, *Member, IEEE*, Luca Sanguinetti, *Senior Member, IEEE*,
Thomas L. Marzetta, *Life Fellow, IEEE*

Abstract

The majority of stochastic channel models rely on the electromagnetic far-field assumption. This assumption breaks down in future applications that push towards the electromagnetic near-field region such as those where the use of very large antenna arrays is envisioned. Motivated by this consideration, we show how physical principles can be used to derive a channel model that is also valid in the electromagnetic near-field. We show that wave propagation through a three-dimensional scattered medium can be generally modeled as a linear and space-variant system. We first review the physics principles that lead to a closed-form deterministic angular representation of the channel response. This serves as a basis for deriving a stochastic representation of the channel in terms of statistically independent Gaussian random coefficients for randomly spatially-stationary propagation environments. The very desirable property of spatial stationarity can always be retained by excluding reactive propagation mechanisms confined in the extreme near-field propagation region. Remarkably, the provided stochastic representation is directly connected to the Fourier spectral representation of a general spatially-stationary random field.

Index Terms

Physical channel modeling, electromagnetic wave propagation, stochastic channel modeling, Fourier spectral representation, angular representation, large antenna arrays, high-frequency communications.

Part of this work was presented at the IEEE International Symposium on Information Theory (ISIT), Vail, CO, 2018 [1] and the Asilomar Conference on signals, Systems and Computers, Pacific Grove, CA, 2021 [2]. A. Pizzo and L. Sanguinetti are with the Dipartimento di Ingegneria dell'Informazione, University of Pisa, 56122 Pisa, Italy (andrea.pizzo@ing.unipi.it, luca.sanguinetti@unipi.it). T.L. Marzetta is with the Department of Electrical and Computer Engineering, Tandon School of Engineering, 11201 Brooklyn, NY (tom.marzetta@nyu.edu).

I. INTRODUCTION

Understanding the foundations of wireless communications systems requires accurate, yet tractable, channel models that reflect their main characteristics and properties. Channel models are either deterministic or stochastic. Deterministic models are very accurate, but valid only for the considered propagation conditions. Unlike deterministic models, stochastic approaches are independent of a particular propagation environment but require a genuine fusion of wave propagation theory with communication and information theory [3]. The incorporation of Maxwell's theory of electromagnetism [4] into Shannon's theory of information [5] may only be possible with the development of a wave theory of information [6], [7]. Attempts in this direction can be found in the literature but only under the assumption that the transport of information by waves occurs with planar wavefronts, i.e., plane-waves. This is true only in the far-field propagation region [8], where angular representations of wireless channels may naturally be found, even in a scattered propagation medium [9]–[14]. However, the electromagnetic far-field assumption breaks down in future applications that push towards the electromagnetic near-field region. An example is represented by communication technologies where the use of very large antenna arrays is envisioned. Research in this direction is taking place under the names of holographic multiple-input-multiple-output (MIMO) [1], [2], [15], [16], large intelligent surfaces [17], and reconfigurable intelligent surfaces [18]–[21], extremely large antenna array apertures [22]. The use of high frequencies (in the range of millimeter-wave and sub-terahertz frequency bands [23], [24]) undermines further the plane-wave assumption.

A. Motivation

Consider wireless transfer of information between two parallel continuous-space arbitrary volumes $V_S \subset \mathbb{R}^3$ and $V_R \subset \mathbb{R}^3$ in a three-dimensional (3D) propagation environment, as depicted in Fig. 1. A scalar electric current density $j(\mathbf{s}) \in \mathcal{L}^2(V_S)$ is applied at the source volume V_S whereas a scalar electric field intensity $e(\mathbf{r}) \in \mathcal{L}^2(V_R)$ is measured at the receive volume V_R . Wireless transfer of information between volumes was studied in [25] under a free-space propagation environment, and extended to the case of pure reflective material objects in [26]. Conversely, we make no prior assumption on the structure of the material objects and assume an arbitrary scattered propagation environment.

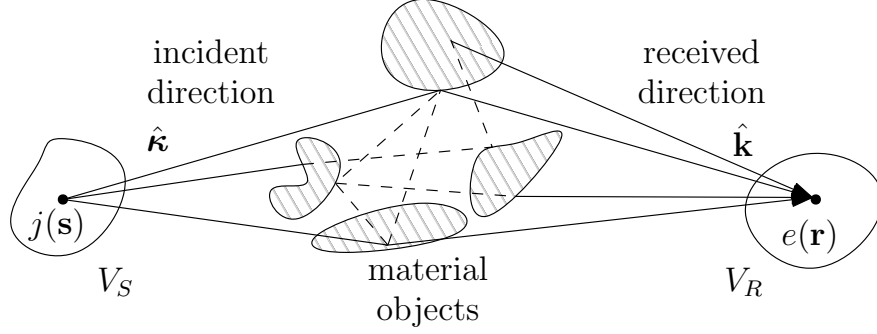


Fig. 1. Schematic diagram of wave propagation between two volumes V_S and V_R in a 3D scattered medium. When the material objects are located in the far-field region of the source and receiver, wave propagation between V_S and V_R can be described in terms of plane-waves.

In a frequency nonselective fading channel, at a particular time instant, the map between the input field $j(\mathbf{s})$ and noise-free output field $e(\mathbf{r}) = (\mathbb{H}j)(\mathbf{r})$ is described by a linear integral operator $\mathbb{H} : \mathcal{L}^2(V_S) \rightarrow \mathcal{L}^2(V_R)$ according to the input-output relationship [11]:

$$e(\mathbf{r}) = \int_{V_S} h(\mathbf{r}, \mathbf{s}) j(\mathbf{s}) d\mathbf{s}, \quad \mathbf{r} \in V_R. \quad (1)$$

Here, the spatial kernel $h(\mathbf{r}, \mathbf{s})$ of the *communication operator* \mathbb{H} can be regarded as the six-dimensional (6D) *space-variant channel response* at point \mathbf{r} due to a unit impulse (point source) applied at point \mathbf{s} .

Elementary treatments of electromagnetic propagation [8] teach that the electric field generated by V_S can be represented by an *incident plane-wave* at any observation point in the far-field region of the source (i.e., at a sufficient number of wavelengths from V_S), as shown in Fig. 2. Changing the observation point, we obtain a continuum of plane-waves propagating from possibly every direction. Upon interaction with the material objects, a continuum of *scattered plane-waves* is measured in the far-field region at any receive point $\mathbf{r} \in V_R$. As illustrated in Fig. 1, the transfer of information between V_S and V_R occurs via a possibly infinite number of propagation directions or *paths*, which is the foundation of multipath channels [9]–[14]. Hence, an exact deterministic angular representation of $h(\mathbf{r}, \mathbf{s})$ in terms of plane-waves – with material objects located in the far-field of both V_S and V_R – is given by

$$h(\mathbf{r}, \mathbf{s}) = \frac{1}{(2\pi)^2} \iiint_{-\infty}^{\infty} a_r(\mathbf{k}, \mathbf{r}) H_a(k_x, k_y, \kappa_x, \kappa_y) a_s(\boldsymbol{\kappa}, \mathbf{s}) d\kappa_x d\kappa_y dk_x dk_y. \quad (2)$$

Particularly, (2) suggests that $h(\mathbf{r}, \mathbf{s})$ can be decomposed into three terms [11]. The first term $a_s(\boldsymbol{\kappa}, \mathbf{s})$ with $\boldsymbol{\kappa} = \kappa_x \hat{\mathbf{x}} + \kappa_y \hat{\mathbf{y}} + \kappa_z \hat{\mathbf{z}}$ is the incident plane-wave that is the *source response* that

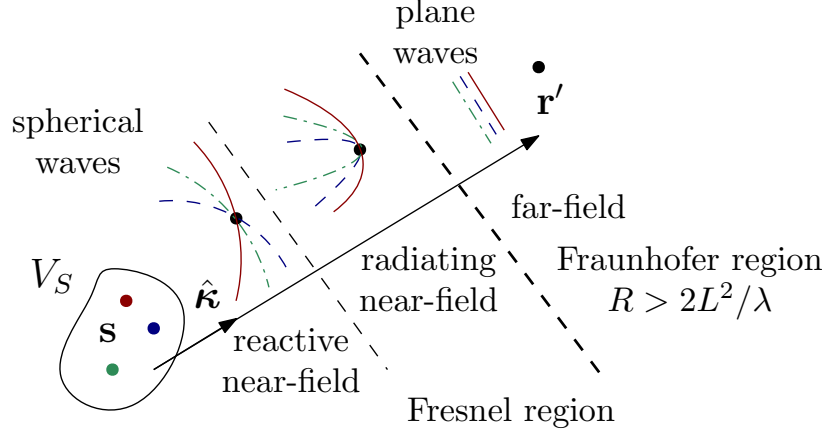


Fig. 2. Near-field (reactive and radiating) and far-field electromagnetic propagation regions. In the reactive near-field region, every point-source applied at $s \in V_S$ generates at r' a spherical wave with different spherical wavefronts. In the radiating near-field region, the effect of evanescent waves vanish; wavefronts are not spherical, but the wavefronts curvature is not negligible to be assumed as locally planar. In the far-field region, perturbing the excitation point s does not change the wavefronts, which are locally planar all with propagation direction $\hat{\kappa}$.

maps the impulsive excitation current at point s to the source propagation direction $\hat{\kappa} = \kappa / \|\kappa\|$ of the incident field. Similarly, the second term $a_r(\mathbf{k}, \mathbf{r})$ with $\mathbf{k} = k_x \hat{\mathbf{x}} + k_y \hat{\mathbf{y}} + k_z \hat{\mathbf{z}}$ is the received plane-wave that is the *receive response* that maps the receive propagation direction $\hat{\mathbf{k}} = \mathbf{k} / \|\mathbf{k}\|$ of the receive field to the induced current at point \mathbf{r} .¹ The third term $H_a(k_x, k_y, \kappa_x, \kappa_y)$ is the *angular response* that maps every incident direction $\hat{\kappa}$ into every other receive direction $\hat{\mathbf{k}}$.

In the proximity of the source, i.e., in the reactive near field, the electric field generated by a point-source at any $s \in V_S$ can be represented by a spherical wave with spherical wavefronts. Hence, the electric field generated by V_S is generally represented by a continuum of spherical waves as illustrated in Fig. 2. It is thus less obvious that an *exact* plane-wave description of the channel response $h(\mathbf{r}, s)$ can always be found even in the reactive near-field region [28]–[30], and for an arbitrary scattered environment, as depicted in Fig. 3.

¹We consider the source $a_s(\kappa, s)$ and receive $a_r(\mathbf{k}, \mathbf{r})$ responses only and neglect the antenna element response. This would require further assumptions on the antenna array implementation, which is not clearly defined for metamaterials [27].

B. Contributions

As anticipated, wave propagation can be generally formulated in terms of plane-waves even in the reactive near-field region [28]–[30]. In Section II, we introduce the electromagnetic wave propagation problem setup given by a general 3D scattered medium as depicted in Fig. 3. We provide a linear-system theoretic interpretation of the wave propagation phenomena and show that it can generally be modeled as a linear and space-variant system with channel response $h(\mathbf{r}, \mathbf{s})$. In Section III, by using tools available from classical optical physics [31]–[33], we review the fundamentals that lead to a deterministic angular representation of $h(\mathbf{r}, \mathbf{s})$ that is valid even in the reactive near-field region in Fig. 2. The plane-waves description of the channel response $h(\mathbf{r}, \mathbf{s})$ apparently coincides to the plane-wave integral representation in (2) that is valid for the far-field regime only. Notice that the integration in (2) is performed on the horizontal coordinates $(k_x, k_y, \kappa_x, \kappa_y)$ only. We will show that this is because the longitudinal coordinates (k_z, κ_z) of a plane-wave are obtained through parametrization from the horizontal coordinates. As observed in [34], the world – at both source and receiver – has only an apparent 3D informational structure, which is subject to a 2D representation. The implication of a reciprocal medium on the angular response $H_a(k_x, k_y, \kappa_x, \kappa_y)$ in (2) are also discussed.

Accurate modeling of $H_a(k_x, k_y, \kappa_x, \kappa_y)$ requires a deep understanding of the underlying physical propagation environment, i.e., the structure and geometry of the material objects. General inferences that abstract from the considered environment are only possible by using stochastic models [1]. This is addressed in Section IV, which extends the work done in [15] considering the receive side only. Here, the channel is modeled as randomly space-variant where each realization is representative of wave propagation into a hypothetically different environment, i.e., $h(\mathbf{r}, \mathbf{s})$ is a spatial random field. We show that the physical implication of a spatial stationarity assumption on $h(\mathbf{r}, \mathbf{s})$ is the restriction of the operating regime to the radiating near-field only in which the wavefronts are not spherical, but the wavefronts curvature is not negligible to be assumed as locally planar; see Fig. 2. In the radiating near-field region, the very desirable property of spatial stationarity can be retained and $h(\mathbf{r}, \mathbf{s})$ can be conveniently modeled as a circularly-symmetric, complex-Gaussian, and stationary spatial random field.

Average transfer of power between every source $\hat{\mathbf{k}}$ and receive $\hat{\mathbf{k}}$ propagation directions is modeled by the variances of $H_a(k_x, k_y, \kappa_x, \kappa_y)$. The modeling of these variances is addressed in Section V where we propose a general enough model for arbitrarily selective propagation

environment that is inspired by directional statistics. In Section VI, we find a Fourier spectral representation of $h(\mathbf{r}, \mathbf{s})$ between every two parallel z -planes at source and receiver, which provides a second-order characterization of the channel in terms of statistically independent Gaussian random coefficients. This representation is built upon the spatial stationarity model developed in Section IV and is valid asymptotically, i.e., when the horizontal measures of V_S and V_R are large enough compared to the wavelength squared.

In Section VII, we extend the deterministic and stochastic frameworks to the more general case illustrated in Fig. 9, where the material objects may be located everywhere in space, i.e., even in the left and right half-spaces of V_S and V_R , respectively. Section VIII shows how the proposed physics-based stochastic channel model generalizes other well-known models already available in the research literature. Interestingly, the Clarke's isotropic model can be found as a particular instance of the proposed plane-wave model, whereas the i.i.d. Rayleigh fading model is strictly speaking incompatible with physics.

C. Notation

We will use upper (lower) case letters for spatial-frequency (spatial) entities. Boldfaced letters are used for vectors and matrices. The superscripts T and * stand for transposition and element-wise conjugation. For two matrices \mathbf{A} and \mathbf{B} of same size, the Hadamard product is denoted as $\mathbf{A} \odot \mathbf{B}$. We use \mathbb{R}^n and \mathbb{C}^n to denote the n -dimensional real-valued and complex-valued Euclidean vector spaces. In general, blackboard bold letters are used to denote integral operators. A general point in the \mathbb{R}^3 Euclidean space is described by the spatial vector $\mathbf{r} = x\hat{\mathbf{x}} + y\hat{\mathbf{y}} + z\hat{\mathbf{z}}$ where $\hat{\mathbf{x}}$, $\hat{\mathbf{y}}$, and $\hat{\mathbf{z}}$ are three orthonormal vectors, and (x, y, z) are its Cartesian coordinates. The length of this vector is $\|\mathbf{r}\| = \sqrt{x^2 + y^2 + z^2}$ and $\hat{\mathbf{r}} = \mathbf{r}/\|\mathbf{r}\|$ is a unit vector that is parallel to \mathbf{r} . $\nabla_R^2 = \frac{\partial^2}{\partial x^2} + \frac{\partial^2}{\partial y^2} + \frac{\partial^2}{\partial z^2}$ is the scalar Laplace operator with respect to the spatial variable \mathbf{r} . Any other set is indicated by using a calligraphic letter \mathcal{X} . In particular, $\mathcal{L}^2(\mathcal{X})$ is the Hilbert space of square-integrable fields defined on \mathcal{X} . The Lebesgue measure of a set \mathcal{X} is indicated by $|\mathcal{X}|$. $\mathbb{1}_{\mathcal{X}}(x)$ is the indicator function that equal 1 in the region $x \in \mathcal{X}$ but is 0 outside this region. The real and imaginary parts of a complex number are $\text{Re}\{\cdot\}$ and $\text{Im}\{\cdot\}$, respectively. $\delta(x)$ is the Dirac delta function while δ_n is the Kronecker delta. $\mathbb{E}\{\cdot\}$ denotes the expectation operator. The notation $n \sim \mathcal{N}_{\mathbb{C}}(0, \sigma^2)$ stands for a circularly-symmetric complex-Gaussian random variable with variance σ^2 .

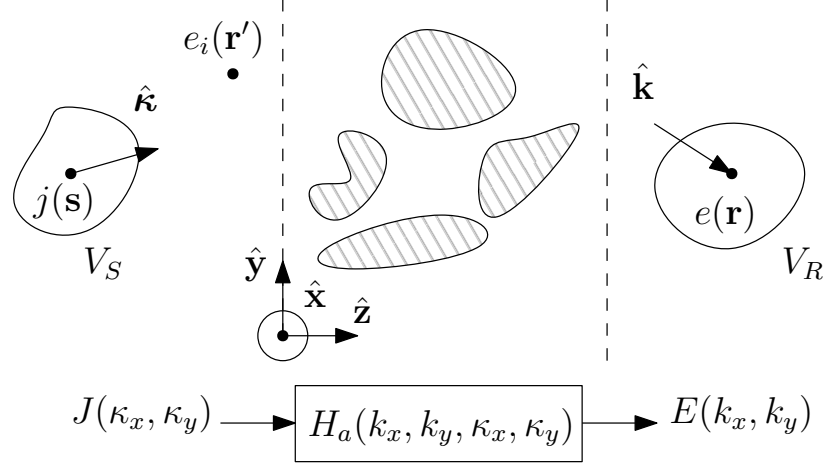


Fig. 3. Schematic diagram of wave propagation between two volumes V_S and V_R in a 3D scattered medium. The electric current density $j(\mathbf{s})$ applied at V_S generates a spectrum $J(\kappa_x, \kappa_y)$ of incident plane-waves. Upon interaction with the material objects separating the two volumes, a spectrum $E(k_x, k_y)$ of scattered plane-waves contribute to the receive electric field $e(\mathbf{r})$ measured at V_R . The scattering mechanism is fully embedded into the angular response $H_a(k_x, k_y, \kappa_x, \kappa_y)$.

II. ELECTROMAGNETIC WAVE PROPAGATION PROBLEM

We assume that electromagnetic propagation between the source V_S and receive V_R volumes takes place in the form of monochromatic scalar waves at radiation frequency ω that propagate through a 3D infinite² and homogeneous medium. This medium is characterized by the scalar frequency- and position-independent permeability μ and permittivity ϵ coefficients or equivalently by its intrinsic impedance $\eta = \sqrt{\mu/\epsilon}$. We assume that the material objects separating V_S and V_R are homogeneous and made up of arbitrary shape and size, as illustrated in Fig. 3. These conditions lead to a *reciprocal* propagation medium [8].

The electromagnetic wave propagation problem can be decoupled in three subproblems, as shown in Fig. 3.

1) *The incident field:* The electric current density $j(\mathbf{r}')$ applied at the source V_S generates an incident electric field $e_i(\mathbf{r}')$ that locally obeys the inhomogeneous Helmholtz equation [8]

$$(\nabla_S^2 + \kappa^2)e_i(\mathbf{r}') = i\kappa\eta j(\mathbf{r}') \quad (3)$$

²If we assume wave propagation into an infinite medium we do not need to specify boundary any conditions.

where $\kappa = \omega/c$ is the wavenumber with c being the speed of light. Any point source $-\delta(\mathbf{r}' - \mathbf{s})$ applied at $\mathbf{s} \in V_S$ generates a scalar spherical-wave that is described by the Green's function [8, Eq. (1.3.34)]

$$g(\mathbf{r}' - \mathbf{s}) = \frac{e^{i\kappa\|\mathbf{r}' - \mathbf{s}\|}}{4\pi\|\mathbf{r}' - \mathbf{s}\|}. \quad (4)$$

Adding together all the point sources within V_S yields (because of the principle of superposition of an electric current)

$$e_i(\mathbf{r}') = - \int_{V_S} i\kappa\eta g(\mathbf{r}' - \mathbf{s}) j(\mathbf{s}) d\mathbf{s}. \quad (5)$$

2) *The received field:* Instead of characterizing the complex interactions between the incident field $e_i(\mathbf{r}')$ and material objects separating V_S and V_R , we focus on the scattered field $e(\mathbf{r})$ measured at V_R . While the incident field is artificially created by the electric sources inside V_S , the received field is due to the electric currents present on the surface of the material objects, which are induced by the impinging incident field [6]. Consequently, $e(\mathbf{r})$ is thus locally source-free [35] and obeys the homogeneous Helmholtz equation [8]

$$(\nabla_R^2 + \kappa^2) e(\mathbf{r}) = 0. \quad (6)$$

In absence of scattering (i.e., free-space propagation), the received field $e(\mathbf{r})$ measured at any $\mathbf{r} \in V_R$ coincides to the incident field $e_i(\mathbf{r}')$ in (5) evaluated at $\mathbf{r}' = \mathbf{r}$, i.e., The input current $j(\mathbf{s})$ and output field $e(\mathbf{r})$ are related by the input-output relationship

$$e(\mathbf{r}) = \int_{V_S} h(\mathbf{r} - \mathbf{s}) j(\mathbf{s}) d\mathbf{s}, \quad \mathbf{r} \in V_R \quad (7)$$

with space-invariant channel response given by

$$h(\mathbf{r} - \mathbf{s}) = -i\kappa\eta g(\mathbf{r} - \mathbf{s}). \quad (8)$$

We can conveniently include the space constraints into the kernel by defining a hypothetical space-variant channel response $h_V(\mathbf{r}, \mathbf{s})$ that is zero outside of the source V_S and receive V_R volumes:

$$h_V(\mathbf{r}, \mathbf{s}) = h(\mathbf{r} - \mathbf{s}) \mathbb{1}_{V_R}(\mathbf{r}) \mathbb{1}_{V_S}(\mathbf{s}) \quad (9)$$

where $\mathbb{1}_{V_R}(\mathbf{r})$ and $\mathbb{1}_{V_S}(\mathbf{s})$ are the indicator functions that equal 1 in the regions $\mathbf{r} \in V_R$ and $\mathbf{s} \in V_S$, respectively, but are 0 outside these regions. Therefore, (7) can be rewritten as

$$e(\mathbf{r}) = \int h_V(\mathbf{r}, \mathbf{s}) j(\mathbf{s}) d\mathbf{s}. \quad (10)$$

In the propagation setup of Fig. 3, the received field $e(\mathbf{r})$ does not coincide to the incident field $e_i(\mathbf{r}')$ but it is rather induced by it through a complicated scattering mechanism. This can be taken into account by properly modeling $h_V(\mathbf{r}, \mathbf{s})$.

3) *The scattering mechanism:* Due to linearity of the Helmholtz equations, the received field $e(\mathbf{r})$ must be linearly related to the incident field $e_i(\mathbf{r}')$ [31], and consequently to $j(\mathbf{s})$ through (5). Hence, even in presence of arbitrary scattering, the input-output relationship is given by (10) after replacing $h(\mathbf{r} - \mathbf{s})$ in (9) with a generalized channel response $h(\mathbf{r}, \mathbf{s})$, i.e.,

$$h_V(\mathbf{r}, \mathbf{s}) = h(\mathbf{r}, \mathbf{s}) \mathbb{1}_{V_R}(\mathbf{r}) \mathbb{1}_{V_S}(\mathbf{s}). \quad (11)$$

From a mathematical point of view, $h_V(\mathbf{r}, \mathbf{s})$ or equivalently $h(\mathbf{r}, \mathbf{s})$, is sufficient to describe the entire wave propagation problem in Fig. 3. From a physical point of view, however, we are often interested in modelling the wave propagation problem as a linear and space-variant (LSV) system [36]. The input-output relationship of this LSV system is obtained from (10) by applying the transformation $\mathbf{s} = \mathbf{r} - \mathbf{p}$:

$$e(\mathbf{r}) = \int c_V(\mathbf{r}, \mathbf{p}) j(\mathbf{r} - \mathbf{p}) d\mathbf{p} \quad (12)$$

where

$$c_V(\mathbf{r}, \mathbf{p}) = c(\mathbf{r}, \mathbf{p}) \mathbb{1}_{V_R}(\mathbf{r}) \mathbb{1}_{V_S}(\mathbf{r} - \mathbf{p}) \quad (13)$$

with $c(\mathbf{r}, \mathbf{p}) = h(\mathbf{r}, \mathbf{r} - \mathbf{p})$ being the channel impulse response measured at point \mathbf{r} due to a unit impulse (point-source) applied at point $\mathbf{r} - \mathbf{p}$.

In the next section, we elaborate each one of the above subproblem separately and put together all results to obtain an exact closed-form expression of $h(\mathbf{r}, \mathbf{s})$ in (11) that is valid for any scattered propagation environment. Elaborating on [28]–[30], we anticipate that the incident field $e(\mathbf{r}')$ is represented by an integral superposition of incident plane-waves, and the received field $e(\mathbf{r})$ is represented by another integral superposition of plane-waves. These two representations are connected by a scattering kernel integral operator that linearly combines all incident plane-waves into every received plane-wave. As a consequence, the electromagnetic wave propagation problem in Fig. 3 can be generally formulated in terms of plane-waves irrespective of the distances among the two volumes V_R and V_S and the material objects, that is, even in the extreme near-field region [28]–[30].

III. PLANE-WAVE REPRESENTATION OF ELECTROMAGNETIC PROPAGATION

As mentioned earlier, elementary treatments of electromagnetic propagation [8] teach that the electric field can be represented with a single plane-wave in the far-field region of the source, i.e., at a sufficient number of wavelengths from the source. Next, we show that the channel response $h(\mathbf{r}, \mathbf{s})$ (and in turn the channel impulse response $c(\mathbf{r}, \mathbf{s})$) can be *exactly* described by the plane-wave integral representation in (2), which is also valid in the extreme near-field region.

A. The incident field

The Green function in (4) describes a scalar spherical-wave that propagates radially from the excitation point \mathbf{s} . The Weyl's identity decomposes any spherical-wave into an uncountably infinite number of plane-waves $e^{i(\kappa_x x + \kappa_y y + \kappa_z z)}$ as [8, Eq. (2.2.27)]

$$\frac{e^{i\kappa R}}{R} = \frac{i}{2\pi} \iint_{-\infty}^{\infty} \frac{e^{i(\kappa_x x + \kappa_y y + \kappa_z z)}}{\kappa_z} d\kappa_x d\kappa_y, \quad z > 0 \quad (14)$$

where $R = \sqrt{x^2 + y^2 + z^2} > 0$ and

$$\kappa_z = \sqrt{\kappa^2 - \kappa_x^2 - \kappa_y^2} \in \mathbb{C} \quad (15)$$

that is parametrized by the other two coordinates $(\kappa_x, \kappa_y) \in \mathbb{R}^2$. At any point $\mathbf{p} = x\hat{\mathbf{x}} + y\hat{\mathbf{y}} + z\hat{\mathbf{z}}$, each plane-wave

$$e^{i(\kappa_x x + \kappa_y y + \kappa_z z)} = e^{i\boldsymbol{\kappa}^T \mathbf{p}} \quad (16)$$

is specified by a source wave vector $\boldsymbol{\kappa} = \kappa_x \hat{\mathbf{x}} + \kappa_y \hat{\mathbf{y}} + \kappa_z \hat{\mathbf{z}}$ with length

$$\|\boldsymbol{\kappa}\| = \sqrt{\kappa_x^2 + \kappa_y^2 + \kappa_z^2} = \kappa. \quad (17)$$

The unit vector

$$\hat{\boldsymbol{\kappa}} = \boldsymbol{\kappa} / \|\boldsymbol{\kappa}\| = \boldsymbol{\kappa} / \kappa \quad (18)$$

describes the propagation direction towards which the plane-wave is travelling from \mathbf{s} . In (14), the negative part $z < 0$ of the spherical-wave solution (4) is discarded since only the upgoing plane-waves travelling towards the upper-hemisphere $+\hat{\mathbf{z}}$ in Fig. 3 are considered. The exclusion of downgoing plane-waves travelling towards the lower-hemisphere $-\hat{\mathbf{z}}$ may be interpreted as a physical *causality* condition. In particular, if no backscattering phenomena occurs at the source, i.e., there is no material object in the left half-space of V_S , downgoing plane-waves do not contribute to the receive field $e(\mathbf{r})$.

Notice that since κ_x and κ_y can vary independently in \mathbb{R}^2 , κ_z in (15) can be either real- or imaginary-valued. In particular, it is real-valued within the support

$$\mathcal{D} = \{(\kappa_x, \kappa_y) \in \mathbb{R}^2 : \kappa_x^2 + \kappa_y^2 \leq \kappa^2\} \quad (19)$$

given by a centered disk of radius κ and imaginary-valued on its complementary set

$$\overline{\mathcal{D}} = \{(\kappa_x, \kappa_y) \in \mathbb{R}^2 : \kappa_x^2 + \kappa_y^2 > \kappa^2\}. \quad (20)$$

Also, κ_z must be such that the incident field obeys the Sommerfeld's radiation condition at infinity (when $z > 0$) for an infinite medium [8], which ensures the convergence of (14). This condition requires that $\text{Re}\{\kappa_z\} \geq 0$ and $\text{Im}\{\kappa_z\} \geq 0$ that in turn implies

$$\kappa_z(\kappa_x, \kappa_y) = \begin{cases} \gamma(\kappa_x, \kappa_y), & (\kappa_x, \kappa_y) \in \mathcal{D} \\ i|\gamma(\kappa_x, \kappa_y)|, & (\kappa_x, \kappa_y) \in \overline{\mathcal{D}} \end{cases} \quad (21)$$

where $\gamma(\kappa_x, \kappa_y)$ is defined as

$$\gamma(\kappa_x, \kappa_y) = \sqrt{\kappa^2 - \kappa_x^2 - \kappa_y^2} \in \mathbb{R}. \quad (22)$$

According to the values assumed by (κ_x, κ_y) the exponential $e^{i(\kappa_x x + \kappa_y y + \kappa_z z)}$ is either an oscillatory or an exponentially decaying function in the hemisphere $+\hat{\mathbf{z}}$. When κ_z is real-valued, the exponential is an oscillating function in z that represents a simple *plane-wave*. Conversely, when κ_z is imaginary-valued, the exponential represents an *evanescent wave* with an exponential decay along the z axis [6], [30] as later on illustrated in Fig. 5. This makes the integration region in (14) limited for practical distances between V_R and V_S . Indeed, evanescent waves are generated by reactive propagation mechanisms taking place in the proximity of the source only [29].

By applying the Weyl's identity in (14) to (4) and using (21), at any point \mathbf{r}' arbitrarily close to the source point \mathbf{s} we obtain

$$g(\mathbf{r}' - \mathbf{s}) = \frac{i}{2(2\pi)^2} \iint_{-\infty}^{\infty} \frac{e^{i\mathbf{\kappa}^T(\mathbf{r}' - \mathbf{s})}}{\kappa_z(\kappa_x, \kappa_y)} d\kappa_x d\kappa_y, \quad r'_z > \max_{V_S} s_z \quad (23)$$

for every $s_z \in V_S$. The use of (23) into (5) provides the following 2D plane-wave representation of the incident field

$$e_i(\mathbf{r}') = \iint_{-\infty}^{\infty} E_i(\kappa_x, \kappa_y) e^{i\mathbf{\kappa}^T \mathbf{r}'} d\kappa_x d\kappa_y, \quad r'_z > \max_{V_S} s_z \quad (24)$$

where the complex amplitude $E_i(\kappa_x, \kappa_y)$ of the incident plane-wave propagating towards $\hat{\mathbf{\kappa}}$ is given by

$$E_i(\kappa_x, \kappa_y) = \frac{1}{(2\pi)^2} \frac{\kappa \eta / 2}{\kappa_z(\kappa_x, \kappa_y)} J(\kappa_x, \kappa_y) \quad (25)$$

with

$$J(\kappa_x, \kappa_y) = \int_{V_S} j(\mathbf{s}) a_s(\boldsymbol{\kappa}, \mathbf{s}) d\mathbf{s} \quad (26)$$

and

$$a_s(\boldsymbol{\kappa}, \mathbf{s}) = e^{-i\boldsymbol{\kappa}^T \mathbf{s}} = e^{-i(\kappa_x s_x + \kappa_y s_y + \kappa_z(\kappa_x, \kappa_y) s_z)}. \quad (27)$$

In the physics literature, representations in the form of (24) are known as *angular representations* [37]–[39]. This is due to the fact that the Cartesian coordinates $(\hat{\kappa}_x, \hat{\kappa}_y, \hat{\kappa}_z)$ of $\hat{\boldsymbol{\kappa}}$ in (18) are representative of a propagation direction. However, since κ_z may be imaginary-valued according to (21), the 2D plane-wave representation of the incident field in (24) generally involves complex angles. This is why a representation in terms of $\boldsymbol{\kappa}$, rather than elevation and azimuth angles, is needed [33]. With this observation in mind, we now determine a 2D plane-wave representation of the received field.

An alternative approach leading to (24)–(25) is taken in [29]. Firstly, the spatial Fourier transform is directly applied to the inhomogeneous Helmholtz equation (3) for an arbitrary current density $j(\mathbf{r}')$ and, secondly, the spatial Fourier inversion is taken with respect to the longitudinal coordinate κ_z .

B. The received field

The homogeneous Helmholtz equation in (6) is an eigenvalue equation of the linear space-invariant Helmholtz operator $(\nabla_R^2 + \kappa^2)$ [8]. The solution of (6) is given by the eigenfunction $e^{i(k_x r_x + k_y r_y + k_z r_z)} = e^{i\mathbf{k}^T \mathbf{r}}$ where

$$k_z(k_x, k_y) = \begin{cases} \gamma(k_x, k_y), & (k_x, k_y) \in \mathcal{D} \\ i|\gamma(k_x, k_y)|, & (k_x, k_y) \in \overline{\mathcal{D}} \end{cases} \quad (28)$$

to satisfy the Sommerfeld's radiation condition at infinity [8]. Hence, every eigenfunction of (6) describes a receive plane-wave with wave vector $\mathbf{k} = k_x \hat{\mathbf{x}} + k_y \hat{\mathbf{y}} + k_z \hat{\mathbf{z}}$ of length

$$\|\mathbf{k}\| = \sqrt{k_x^2 + k_y^2 + k_z^2} = \kappa. \quad (29)$$

Hence, the unit vector

$$\hat{\mathbf{k}} = \mathbf{k}/\|\mathbf{k}\| = \mathbf{k}/\kappa \quad (30)$$

describes the propagation direction from which the plane-wave is impinging to \mathbf{r} . The general solution of (6) is obtained by considering the entire eigenspace spanned by these eigenfunctions [15], i.e., an integral superposition of propagating and evanescent plane-waves having arbitrary

complex amplitudes $E(k_x, k_y)$ with $(k_x, k_y) \in \mathbb{R}^2$. This yields the following 2D plane-wave representation for the received field

$$e(\mathbf{r}) = \iint_{-\infty}^{\infty} E(k_x, k_y) a_r(\mathbf{k}, \mathbf{r}) dk_x dk_y, \quad \mathbf{r} \in V_R \quad (31)$$

where

$$a_r(\mathbf{k}, \mathbf{r}) = e^{i\mathbf{k}^T \mathbf{r}} = e^{i(k_x r_x + k_y r_y + k_z(k_x, k_y) r_z)}. \quad (32)$$

Similarly to (24), evanescent waves appear when $(k_x, k_y) \in \overline{\mathcal{D}}$ so that (32) becomes an exponentially decaying function in the upper-hemisphere $+\hat{\mathbf{z}}$. Unlike $E_i(\kappa_x, \kappa_y)$ that depends deterministically on $j(\mathbf{s})$ through (25), the exact values of $E(k_x, k_y)$ are generally not known as they depend on $E_i(\kappa_x, \kappa_y)$ through the underlying scattering mechanism.

In summary, the sole action of a volume source V_S is to create a scalar incident plane-wave spectrum $E_i(\kappa_x, \kappa_y)$. At the receiver, the receive volume V_R measures a scalar receive plane-wave spectrum $E(k_x, k_y)$ [28]. Next, we show how these two spectrum are connected in general. The presented formulation leads to a single 4D plane-wave representation that embeds the two 2D plane-wave representations in (24) and (31), which is valid for an arbitrary scattered propagation environment.

C. The scattering mechanism

Physically, any plane-wave from receive propagation direction $\hat{\mathbf{k}}$ is the result of the interaction between *all* plane-waves propagating towards $\hat{\mathbf{k}}$ spanning the upper-hemisphere $+\hat{\mathbf{z}}$ and material objects. Hence, in general, each receive plane-wave amplitude $E(k_x, k_y)$ is induced by all the incident plane-wave amplitudes $E_i(\kappa_x, \kappa_y)$ with $(\kappa_x, \kappa_y) \in \mathbb{R}^2$ through a functional, which completely describes the scattering mechanism. As a consequence of the linearity of Helmholtz equations, this functional must be linear [31] and each $E(k_x, k_y) = (\mathbb{K}E_i)(k_x, k_y)$ must be obtained as an integral superposition of all $E_i(\kappa_x, \kappa_y)$ through a linear integral operator $\mathbb{K} : \mathcal{L}^2(\mathbb{R}^2) \rightarrow \mathcal{L}^2(\mathbb{R}^2)$ [31], [32]

$$E(k_x, k_y) = \iint_{-\infty}^{\infty} K(k_x, k_y, \kappa_x, \kappa_y) E_i(\kappa_x, \kappa_y) d\kappa_x d\kappa_y \quad (33)$$

where $K(k_x, k_y, \kappa_x, \kappa_y)$ is the kernel of the *scattering operator* \mathbb{K} . From the energy conservation law, $K(k_x, k_y, \kappa_x, \kappa_y)$ is of unit energy as wave propagation takes place into a lossless medium [32]. Since this kernel turns the entire incident plane-wave amplitudes $E_i(\kappa_x, \kappa_y)$ with $(\kappa_x, \kappa_y) \in \mathbb{R}^2$ into each one of the receive plane-wave amplitudes $E(k_x, k_y)$, it can be regarded as a

generalized transmission coefficient [33]. In a free-space scenario (i.e., no material objects), each incident plane-wave reaches the receiver unaltered such that the propagation directions are exactly the same, i.e., $\hat{\mathbf{k}} = \hat{\mathbf{\kappa}}$. The scattering kernel is thus

$$K(k_x, k_y, \kappa_x, \kappa_y) = \delta(k_y - \kappa_y)\delta(k_x - \kappa_x) \quad (34)$$

for $(k_x, k_y, \kappa_x, \kappa_y) \in \mathbb{R}^2 \times \mathbb{R}^2$. By substituting (34) into (33) yields $E(\kappa_x, \kappa_y) = E_i(\kappa_x, \kappa_y)$, as it should be.

In this paper, we will never attempt to physically model the scattering kernel but will rather develop in Section V a sufficiently general model for wave propagation into an arbitrary scattered propagation environment.

D. 4D Fourier plane-wave representation

Plugging (25) into the scattering kernel operator (33) yields $E(k_x, k_y) = (\mathbb{A}J)(k_x, k_y)$ with linear integral operator $\mathbb{A} : \mathcal{L}^2(\mathbb{R}^2) \rightarrow \mathcal{L}^2(\mathbb{R}^2)$ such that

$$E(k_x, k_y) = \frac{1}{(2\pi)^2} \iint_{-\infty}^{\infty} H_a(k_x, k_y, \kappa_x, \kappa_y) J(\kappa_x, \kappa_y) d\kappa_x d\kappa_y \quad (35)$$

where $H_a(k_x, k_y, \kappa_x, \kappa_y)$ is the kernel of the *angular operator* \mathbb{A} defined as

$$H_a(k_x, k_y, \kappa_x, \kappa_y) = \frac{\kappa\eta}{2} \frac{K(k_x, k_y, \kappa_x, \kappa_y)}{\kappa_z(\kappa_x, \kappa_y)}. \quad (36)$$

The substitution of (35) and (26) into (31) yields (10) by defining $h_V(\mathbf{r}, \mathbf{s})$ as in (11) with $h(\mathbf{r}, \mathbf{s})$ given by (2). Here, $a_s(\boldsymbol{\kappa}, \mathbf{s})$ and $a_r(\mathbf{k}, \mathbf{r})$ are the incident and received plane-waves defined earlier. In summary, the sole action of the source $a_s(\boldsymbol{\kappa}, \mathbf{s})$ and receive $a_r(\mathbf{k}, \mathbf{r})$ responses is to change domain of representation, i.e., from spatial to angular and viceversa. Everything else is embedded into the angular response $H_a(k_x, k_y, \kappa_x, \kappa_y)$ that fully describes the underlying physical propagation mechanism angularly. Notice that the dependance of $H_a(k_x, k_y, \kappa_x, \kappa_y)$ on k_z and κ_z is embedded into the horizontal variables (k_x, k_y) and (κ_x, κ_y) through (21) and (28), respectively.

The input-output relationship (10) in the spatial domain should be compared to its angular counterpart in (35). Similarly to $h(\mathbf{r}, \mathbf{s})$ in (11), $H_a(k_x, k_y, \kappa_x, \kappa_y)$ in (35) is the *angular response* at propagation direction $\hat{\mathbf{k}}$ due to a single plane-wave radiated from direction $\hat{\mathbf{\kappa}}$.

In general, $K(k_x, k_y, \kappa_x, \kappa_y)$, and thus, $H_a(k_x, k_y, \kappa_x, \kappa_y)$ can have arbitrary structure. If the medium is reciprocal, however, as assumed in Section II, the electromagnetic reciprocity principle must hold. This imposes the following symmetric structure of the angular response.

Theorem 1. *If the propagation medium is reciprocal, the angular response in (2) must be of the form*

$$H_a(k_x, k_y, \kappa_x, \kappa_y) = \frac{\kappa\eta}{2} \frac{K_a(k_x, k_y, \kappa_x, \kappa_y)}{k_z^{1/2}(k_x, k_y)\kappa_z^{1/2}(\kappa_x, \kappa_y)} \quad (37)$$

with $K_a(\cdot)$ being an arbitrary complex-symmetric kernel as defined in (123).

Proof. The proof is given in Appendix A and follows similar arguments valid for the scalar Green function [8]. \square

As anticipated, (2) with (37) provide to an exact and physically-tenable integral representation of $h(\mathbf{r}, \mathbf{s})$. This is valid irrespective of the distances among the two volumes V_R and V_S and the material objects, that is, even in the extreme near-field region, and under arbitrary propagation conditions. We call (2) with (37) the *4D Fourier plane-wave representation* of $h(\mathbf{r}, \mathbf{s})$ since it exactly describes the channel response as an integral superposition of incident and received plane-waves. The connection between plane-waves and Fourier theory will be investigated next.

Before doing that, we also notice that (23) can be obtained from (2) by imposing $K_a(k_x, k_y, \kappa_x, \kappa_y)$ in Theorem 1 to be impulsive of the form specified in (34). Hence, (2) can be regarded as a *generalized* Weyl's identity that is valid under arbitrary propagation conditions.

E. System functions for LSV channels

For any fixed s_z and $r_z > s_z$, the incident and received plane-waves in (27) and (32) take the form

$$a_s(\boldsymbol{\kappa}, \mathbf{s}) = \phi(\kappa_x, \kappa_y, s_x, s_y) e^{-i\kappa_z(\kappa_x, \kappa_y)s_z} \quad (38)$$

$$a_r(\mathbf{k}, \mathbf{r}) = \phi^*(k_x, k_y, r_x, r_y) e^{ik_z(k_x, k_y)r_z} \quad (39)$$

which correspond to two phase-shifted versions of 2D spatial-frequency Fourier harmonics,³⁴ i.e.,

$$\phi(\xi_x, \xi_y, p_x, p_y) = e^{-i(\xi_x p_x + \xi_y p_y)}. \quad (40)$$

³The change of sign in the plane-wave harmonics at the receiver is because they are incoming at receive point \mathbf{r} . On the other hand, the incident plane-wave harmonics at the source are outgoing from source point \mathbf{s} .

⁴Due to the connection between plane-waves and 2D Fourier harmonics, we will refer to the spatial-frequency or angular domains indistinctly.

The equivalence between the plane-waves in (38) and (39) and 2D Fourier harmonics in (40) leads to a *4D Fourier representation* of the channel response $h(\mathbf{r}, \mathbf{s})$. This is given by

$$h(\mathbf{r}, \mathbf{s}) = \frac{1}{(2\pi)^2} \iiint_{-\infty}^{\infty} \phi^*(k_x, k_y, r_x, r_y) H(k_x, k_y, \kappa_x, \kappa_y; r_z, s_z) \phi(\kappa_x, \kappa_y, s_x, s_y) d\kappa_x d\kappa_y dk_x dk_y \quad (41)$$

which is obtained by using (38) and (39) into (2) where

$$H(k_x, k_y, \kappa_x, \kappa_y; r_z, s_z) = H_a(k_x, k_y, \kappa_x, \kappa_y) e^{i(\kappa_z(k_x, k_y)r_z - \kappa_z(\kappa_x, \kappa_y)s_z)}. \quad (42)$$

The obtained integral representation should be compared to the equivalent 4D Fourier plane-wave representation of $h(\mathbf{r}, \mathbf{s})$ in (2). In analogy with plane-waves in (2), $\phi(\kappa_x, \kappa_y, s_x, s_y)$ and $\phi^*(k_x, k_y, r_x, r_y)$ in (41) change the domain of representation from *spatial* to *spatial-frequency*, and vice-versa, respectively. The entire Fourier characterization of the channel is embedded into $H(k_x, k_y, \kappa_x, \kappa_y; r_z, s_z)$, say the *spectral response* of the channel at spatial-frequency (k_x, k_y) due to an oscillating input at spatial-frequency (κ_x, κ_y) , i.e., $(2\pi)^2 \delta(\kappa'_x - \kappa_x) \delta(\kappa'_y - \kappa_y)$.

The expression of $H(k_x, k_y, \kappa_x, \kappa_y; r_z, s_z)$ in (42) shows that is obtained as the product of the angular response in (36) and a phase response $e^{i(\kappa_z(k_x, k_y)r_z - \kappa_z(\kappa_x, \kappa_y)s_z)}$. The former maps the source to the receiver angularly while the latter accounts for the propagation phase-delay due to communications between different z -planes. In physics, this latter operation is also known as spectral propagator [8] or migration filter [29], [40] and it can be determined a priori as long as the z displacement between the source and receive locations is known. This electromagnetic physical effect can be connected to the Hyugens's equivalent representation of a volume source as an equivalent planar source [29].

Notice that $H(k_x, k_y, \kappa_x, \kappa_y; r_z, s_z)$ describes the spatial-frequency input-output relation for a physical channel. However, when the channel is viewed as a LSV filter as in (12) a *spatial-frequency response* $C(k_x, k_y, \kappa_x, \kappa_y; r_z, s_z)$ of $c(\mathbf{r}, \mathbf{s})$ is more satisfactory. This is related to the channel impulse response $c(\mathbf{r}, \mathbf{s})$ in (13) according to the same spatial-frequency Fourier relationship between $H(k_x, k_y, \kappa_x, \kappa_y; r_z, s_z)$ and $h(\mathbf{r}, \mathbf{s})$, i.e.,

$$H(k_x, k_y, \kappa_x, \kappa_y; r_z, s_z) = \iiint_{-\infty}^{\infty} \phi(k_x, k_y, r_x, r_y) h(\mathbf{r}, \mathbf{s}) \phi^*(\kappa_x, \kappa_y, s_x, s_y) ds_x ds_y dr_x dr_y. \quad (43)$$

A similar relation to (13) can be obtained in the spatial-frequency Fourier domain as

$$C(k_x, k_y, \kappa_x, \kappa_y; r_z, s_z) = H(k_x - \kappa_x, k_y - \kappa_y, -\kappa_x, -\kappa_y; r_z, r_z - s_z). \quad (44)$$

Hence, $C(k_x, k_y, \kappa_x, \kappa_y; r_z, s_z)$ may be regarded as the spectral response of the channel at spatial-frequency (k_x, k_y) above the oscillating input.

In general, the dispersion of the fading channel may be equivalently described in the spatial and/or spatial-frequency domains. Starting from the channel impulse response $c(\mathbf{r}, \mathbf{s})$ we may define 2^4 possible system functions by exploiting the duality between the spatial (r_x, r_y, s_z, s_y) and spatial-frequency $(k_x, k_y, \kappa_x, \kappa_y)$ coordinates for every fixed (r_z, s_z) . Therefore, a mixed dual description of the channel can always be found at convenience [36].⁵ In analogy with the temporal-frequency description of fading channel [41], two more system functions may be of particular interest, i.e., $C(\mathbf{r}, \kappa_x, \kappa_y; s_z)$ and $C(k_x, k_y, \mathbf{s}; r_z)$. The former is defined as

$$C(\mathbf{r}, \kappa_x, \kappa_y; s_z) = \iint_{-\infty}^{\infty} c(\mathbf{r}, \mathbf{s}) \phi^*(\kappa_x, \kappa_y, s_x, s_y) ds_x ds_y \quad (45)$$

which is the spatial response of the channel measured at \mathbf{r} due to the oscillating input at spatial-frequency (κ_x, κ_y) , i.e., $(2\pi)^2 \delta(\kappa'_x - \kappa_x) \delta(\kappa'_y - \kappa_y)$. The latter is instead given by

$$C(k_x, k_y, \mathbf{s}; r_z) = \iint_{-\infty}^{\infty} c(\mathbf{r}, \mathbf{s}) \phi(k_x, k_y, r_x, r_y) dr_x dr_y \quad (46)$$

which describes the spectral response of the channel at spatial-frequency (k_x, k_y) due to a unit impulse (point-source) applied at point $\mathbf{r} - \mathbf{s}$.

IV. STATISTICAL CHARACTERIZATION OF SPATIALLY-STATIONARY GAUSSIAN SCATTERING

In the above section, we have shown that the electromagnetic wave propagation problem in Fig. 3 can exactly be described by the physics-based 4D Fourier plane-wave representation of $h(\mathbf{r}, \mathbf{s})$ in Theorem 1. The entire scattering mechanism is embedded into the angular response $H_a(k_x, k_y, \kappa_x, \kappa_y)$, which is determined by the scattering kernel $K_a(k_x, k_y, \kappa_x, \kappa_y)$ through (37). Accurate modeling of $K_a(k_x, k_y, \kappa_x, \kappa_y)$ requires a deep understanding of the underlying physical propagation environment, that is, the structure and geometry of the material objects and would make it valid for the considered environment only. Hence, general inferences that abstract from the considered environment are only possible by using stochastic models [1].

We thus model $K_a(k_x, k_y, \kappa_x, \kappa_y)$ as random with each realization being representative of wave propagation into a hypothetically different environment. Consequently, the fading channel $h(\mathbf{r}, \mathbf{s})$ becomes a 6D *spatial random field*. In general, a random channel has a mixed deterministic

⁵The ambiguity resulting from using the same letter with an upper-case notation to indicate every such function is typically resolved by the context in which these functions are used.

and random behavior so that the channel response is composed of a purely deterministic, i.e., its mean value, and a zero-mean random components [36]. The former is due to the free-space propagation component of the received field, whereas the latter is created by the induced currents on the surface of the material objects and models a purely scattered propagation component. We assume that there is no direct path connecting source and receiver and model $h(\mathbf{r}, \mathbf{s})$ as a circularly-symmetric, complex-Gaussian, and stationary spatial random field.⁶

The Gaussian assumption often arises as a *diffusion approximation* of the scattering mechanism [42]. In particular, when the distance between scattering events is large compared to the wavelength λ , but small compared to the distance between source V_S and receive V_R volumes, wave propagation becomes diffusive and the values assumed by $h(\mathbf{r}, \mathbf{s})$ are governed by a jointly Gaussian distribution.

The spatial stationarity assumption on $h(\mathbf{r}, \mathbf{s})$ simplifies the analysis as it happens for time-domain stationary Gaussian processes for which we can always find integral or series representations that provide a second-order characterization in terms of statistically independent Gaussian random coefficients [43]. We anticipate that the physical implication of a spatial stationarity assumption on $h(\mathbf{r}, \mathbf{s})$ is the restriction of the operating regime to the radiating near-field only as illustrated in Fig.2.

A. Statistical characterization of the angular response

Under the above Gaussian assumption, the linearity of the Fourier plane-wave representation in (2) implies that each sample of the scattering kernel $K_a(k_x, k_y, \kappa_x, \kappa_y)$ must be a circularly-symmetric and complex-Gaussian random variable. Hence, it can be generally rewritten as

$$K_a(k_x, k_y, \kappa_x, \kappa_y) = A(k_x, k_y, \kappa_x, \kappa_y)W(k_x, k_y, \kappa_x, \kappa_y) \quad (47)$$

where $A(k_x, k_y, \kappa_x, \kappa_y)$ is an arbitrary real-valued, non-negative function that accounts for the angular selectivity of the channel, and $W(k_x, k_y, \kappa_x, \kappa_y)$ is a collection of circularly-symmetric and complex-Gaussian random variables with unit variances. As specified in Theorem 1, $K_a(k_x, k_y, \kappa_x, \kappa_y)$ is a complex-symmetric function in the sense of (123) due to the electromagnetic reciprocity discussed in Appendix A. This requires that also $A(k_x, k_y, \kappa_x, \kappa_y)$ and $W(k_x, k_y, \kappa_x, \kappa_y)$ are complex-symmetric.

⁶We generally refer to stationary random fields since strict stationarity and stationarity in the wide-sense coincides when the field has Gaussian distribution. Notice that we assume stationarity in both variables \mathbf{r} and \mathbf{s} .

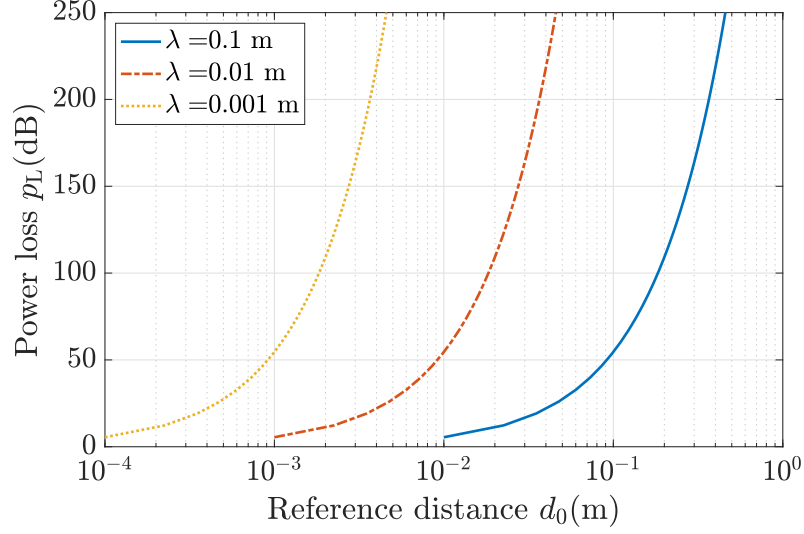


Fig. 4. Power loss in dB of evanescent waves (compared to propagating waves) traveling towards $\hat{\mathbf{z}}$ for $\lambda \in \{0.1, 0.01, 0.001\}$ m.

In (47), $A(k_x, k_y, \kappa_x, \kappa_y)$ physically accounts for the power transfer between incident $\hat{\mathbf{k}}$ and receive $\hat{\mathbf{k}}$ propagation directions in all realizations of $K_a(k_x, k_y, \kappa_x, \kappa_y)$, while $W(k_x, k_y, \kappa_x, \kappa_y)$ allows for changes among realizations due to wave propagation in different environments. Both model microscopic effects caused by small variations in the propagation environment. A sufficient condition on the angular response $H_a(k_x, k_y, \kappa_x, \kappa_y)$ to retain spatial stationarity is given next.

Theorem 2. *If $h(\mathbf{r}, \mathbf{s})$ is a spatially-stationary, circularly-symmetric and complex-Gaussian random field, the angular response in (13) must be of the form*

$$H_a(k_x, k_y, \kappa_x, \kappa_y) = \frac{\kappa\eta}{2} \frac{A(k_x, k_y, \kappa_x, \kappa_y)W(k_x, k_y, \kappa_x, \kappa_y)}{\gamma^{1/2}(k_x, k_y)\gamma^{1/2}(\kappa_x, \kappa_y)} \quad (48)$$

where $(k_x, k_y, \kappa_x, \kappa_y) \in \mathcal{D} \times \mathcal{D}$ with \mathcal{D} being the centered disk of radius κ given in (19) and $W(k_x, k_y, \kappa_x, \kappa_y)$ is a collection of unit-variance, independent and identically distributed (i.i.d.) circularly-symmetric and complex-Gaussian random variables, i.e.,

$$W(k_x, k_y, \kappa_x, \kappa_y) \sim \mathcal{N}_{\mathbb{C}}(0, 1). \quad (49)$$

Proof. The proof is given in Appendix B. We refer to the proof of Lemma 2 in Section VI for the study of the convergence in the mean-squared sense of the stochastic integral representation to the actual channel field $h(\mathbf{r}, \mathbf{s})$. \square

The spatial stationarity assumption on $h(\mathbf{r}, \mathbf{s})$ leads to an *uncorrelated scattering* model for the angular response $H_a(k_x, k_y, \kappa_x, \kappa_y)$ whose autocorrelation function is proportional to a Dirac delta function in the angular domain, i.e., the angular response of one pair of directions $(\hat{\mathbf{k}}, \hat{\kappa})$ is uncorrelated to another pair $(\hat{\mathbf{k}}', \hat{\kappa}')$. Uncorrelated scattering models have been widely used in the research literature, e.g., [9], [10], [12]. However, the physical implications of using this type of models have never been discussed elsewhere, as also observed in [44]. Theorem 2 states that this model is a direct consequence of the spatial stationarity assumption.

Moreover, it shows that the angular response $H_a(k_x, k_y, \kappa_x, \kappa_y)$ must be defined over the compact support given by $(k_x, k_y, \kappa_x, \kappa_y) \in \mathcal{D} \times \mathcal{D}$, which implies the exclusion of evanescent waves from our analysis generated by the source and induced current on the material objects. These waves have imaginary-valued κ_z and k_z as given by (21) and (28), respectively. Hence, they are associated to reactive propagation mechanisms only [29]. This condition implies that spatial stationarity of $h(\mathbf{r}, \mathbf{s})$ can always be retained at a sufficient number of wavelengths from the source and scatterers. In Fig. 4, we quantify the power loss in dB of evanescent waves (compared to propagating waves) traveling towards $\hat{\mathbf{z}}$ for $\lambda \in \{0.1, 0.01, 0.001\}$ m. For a reference distance d_0 (in units of m) between any pair of source and receive points, this is given by

$$p_L(d_0) = e^{-2|\gamma(0,0)|d_0} = e^{-4\pi d_0/\lambda} \quad (50)$$

where we have used $\gamma(\cdot)$ in (22) and $\kappa = 2\pi/\lambda$. We see that when $d_0 \geq 10\lambda$ the power loss is hundreds of dB, and thus, the contribution to evanescent waves is practically null.

B. Spectral characteristics of stationary channels

Consider now the implications of Theorem 2 on the spectral response $H(k_x, k_y, \kappa_x, \kappa_y; r_z, s_z)$ in (42). Due to stationarity, the spatial frequency harmonics of $\phi^*(\kappa_x, \kappa_y, s_x, s_y)$ and $\phi(k_x, k_y, r_x, r_y)$ outside of the support $\mathcal{D} \times \mathcal{D}$ are cut out. Hence, as illustrated in Fig. 5, $H(k_x, k_y, \kappa_x, \kappa_y; r_z, s_z)$ is *circularly band-limited* in both spatial variables \mathbf{r} and \mathbf{s} , each one of which is of bandwidth

$$\Omega_{\text{iso}} = |\mathcal{D}| = \pi\kappa^2 \quad (51)$$

given by the Lebesgue measure of its spectral support \mathcal{D} in (19). Accordingly, the channel can be viewed as an LSV filter in both spatial variables \mathbf{r} and \mathbf{s} with spatial-frequency response $C(k_x, k_y, \kappa_x, \kappa_y; r_z, s_z)$ defined in (44). In doing so, a stationary channel acts as a (baseband) LSV physical *low-pass filter* with spatial-frequency bandwidth given by (51).

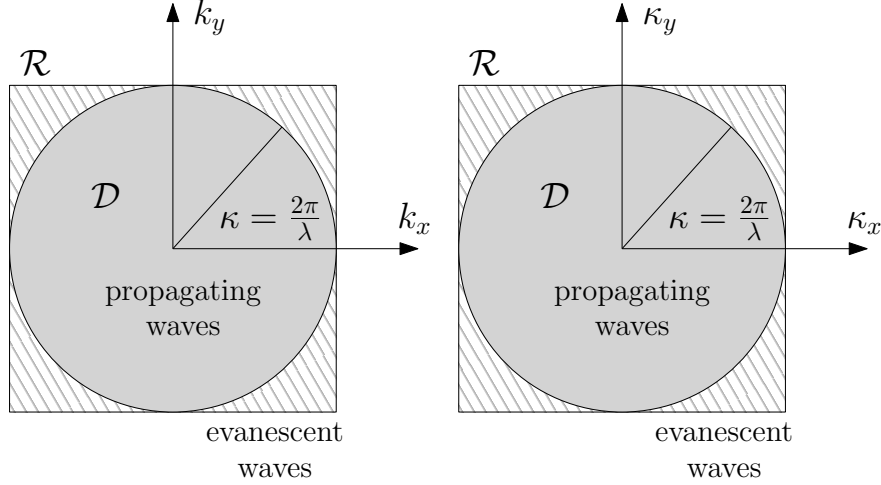


Fig. 5. The channel response $h(\mathbf{r}, \mathbf{s})$ of a spatially-stationary propagation medium behaves as a (baseband) lowpass filter that cuts out all spatial frequencies outside of the circularly bandlimited support $(k_x, k_y, \kappa_x, \kappa_y) \in \mathcal{D} \times \mathcal{D}$.

The above spatial-frequency bandwidth Ω_{iso} is achieved when $A(k_x, k_y, \kappa_x, \kappa_y)$ in (48) is nonzero over its entire support $\mathcal{D} \times \mathcal{D}$. As a particular case, it is worth mentioning the *isotropic* propagation environment [15] wherein transfer of power between V_S and V_R is uniformly distributed on every propagation directions $\hat{\mathbf{k}}$ and $\hat{\mathbf{\kappa}}$; see Fig. 8a. Since the radial dimension of \mathcal{D} is given by $\kappa = \omega/c = 2\pi/\lambda$, the channel's bandwidth Ω_{iso} is inversely proportional to the square of wavelength, i.e., $\propto 1/\lambda^2$. In other words, the lower the wavelength λ , the larger the spatial-frequency bandwidth Ω_{iso} .

In a realistic propagation environment, however, transfer of power between source and receiver occurs through a finite number N_c of angular regions $\Theta_{r,i} \times \Theta_{s,i}$ with $i = 1, \dots, N_c$, each one of which is subtended by the i -th cluster of material objects. Hence, $A(k_x, k_y, \kappa_x, \kappa_y)$ will only be nonzero on these N_c angular regions, as graphically illustrated in Fig. 8b and Fig. 8c. We refer to Section V for a comprehensive description of the angular transfer of power. The size of the union of these angular regions $\Theta_{r,i} \times \Theta_{s,i}$ determines the available spatial-frequency bandwidth Ω at source and receiver for an arbitrary propagation environment. This is given by the Lebesgue measure (e.g., at the source)

$$\Omega = \left| \bigcup_{i=1}^{N_c} \Theta_{s,i} \right|. \quad (52)$$

Clearly, Ω is upper bounded by Ω_{iso} in (51), i.e., $\Omega \leq \Omega_{\text{iso}}$, which is therefore the *maximum achievable bandwidth*. In turn, decreasing the wavelength λ will have no effect on the available

bandwidth Ω , which is fundamentally limited by the physical properties of the propagation environment.

Similarly to time-domain channels, the amount of information that can be transferred into space-domain channels is fundamentally limited by the available (baseband) bandwidth Ω . As an example, for a channel of frequency bandwidth $B/2\pi$ and observed over a time interval of duration T , the BT/π Shannon's formula [45] specifies the number of parallel channels that can be established between a source and receiver, i.e., the channel degrees of freedom (DoF). The spatial counterpart to the BT/π formula for a channel observed over a 1D spatial segment of length L is given by $\Omega L/\pi$ [6], [11], [46]. Hence, in transferring information wirelessly in a stationary channel between two spatial segments we do not incur in any loss. This can be graphically inspected by Fig. 5 where the κ_x and k_x supports are fully enclosed within the spectral support $\mathcal{D} \times \mathcal{D}$. This is not true when we consider planar or volumetric rectangular regions of arbitrary side length L . In the 2D isotropic case, e.g., we have a loss in terms of DoF given by the ratio between the Lebesgue measures of \mathcal{D} and its circumscribing square \mathcal{R} at both source and receiver, i.e., [46]

$$\frac{\Omega_{\text{iso}}}{(2\kappa)^2} = \frac{\pi}{4} < 1 \quad (53)$$

which represents the price we must pay when adding another spatial dimensions. This is again due to stationarity since we excluded the communication modes carried by the evanescent waves. The expansion of a 2D rectangular region into a 3D volumetric region yields no gain in terms of DoF [46].

C. Power spectral density

For a zero-mean, spatially-stationary and complex-Gaussian random field $h(\mathbf{r}, \mathbf{s})$, the spatial autocorrelation function

$$c_h(\mathbf{r}, \mathbf{s}) = \mathbb{E}\{h^*(\mathbf{r}', \mathbf{s}')h(\mathbf{r}' + \mathbf{r}, \mathbf{s}' + \mathbf{s})\} \quad (54)$$

computed for every pair of points $(\mathbf{r}', \mathbf{s}')$ and $(\mathbf{r}' + \mathbf{r}, \mathbf{s}' + \mathbf{s})$ provides a complete statistical description of the field in the spatial domain. Plugging the 4D Fourier plane-wave representation (2) with (48) into (54) yields

$$c_h(\mathbf{r}, \mathbf{s}) = \frac{1}{(2\pi)^4} \iiint\limits_{-\infty}^{\infty} a_r(\mathbf{k}, \mathbf{r}) S(k_x, k_y, \kappa_x, \kappa_y) a_s(\boldsymbol{\kappa}, \mathbf{s}) d\kappa_x d\kappa_y dk_x dk_y \quad (55)$$

where

$$S(k_x, k_y, \kappa_x, \kappa_y) = \left(\frac{\kappa\eta}{2}\right)^2 \frac{A^2(k_x, k_y, \kappa_x, \kappa_y)}{\gamma(k_x, k_y)\gamma(\kappa_x, \kappa_y)} \quad (56)$$

is defined over $(k_x, k_y, \kappa_x, \kappa_y) \in \mathcal{D} \times \mathcal{D}$. In analogy with (2), (55) can be seen as the 4D Fourier plane-wave representation of the spatial autocorrelation function $c_h(\mathbf{r}, \mathbf{s})$. By recalling the connection between plane-waves and 2D Fourier harmonics in (38) and (39), we notice that source $a_s(\boldsymbol{\kappa}, \mathbf{s})$ and receive $a_r(\mathbf{k}, \mathbf{r})$ plane-waves constitute two orthonormal Fourier basis set of functions on every pair of infinite z -planes at source and receiver, respectively. It thus follows that (55) can be regarded as the Hilbert-Schmidt decomposition of the self-adjoint kernel $c_h(\mathbf{r}, \mathbf{s})$ [47]. The 4D spectral function $S(k_x, k_y, \kappa_x, \kappa_y)$ in (56) is different from the classical power spectral density $S(k_x, k_y, k_z, \kappa_x, \kappa_y, \kappa_z)$ defined for any spatially-stationary random field. The latter is related to $c_h(\mathbf{r}, \mathbf{s})$ through the 6D inverse spatial-frequency Fourier transform due to the Wiener-Kintchine theorem, i.e.,

$$c_h(\mathbf{r}, \mathbf{s}) = \iiint\limits_{-\infty}^{\infty} \iiint\limits_{-\infty}^{\infty} S(k_x, k_y, k_z, \kappa_x, \kappa_y, \kappa_z) e^{i(k_x r_x + k_y r_y + k_z r_z)} e^{-i(\kappa_x s_x + \kappa_y s_y + \kappa_z s_z)} dk_x dk_y dk_z d\kappa_x d\kappa_y d\kappa_z. \quad (57)$$

To comply with (41), we have changed the sign in the spatial-frequency coordinates at the source with respect to the ordinary inverse Fourier transform. As shown for the source-free case in [1], [15], the structure of $S(k_x, k_y, k_z, \kappa_x, \kappa_y, \kappa_z)$ in (57) under arbitrary stationary propagation conditions is impulsive defined on a centered sphere of radius κ and is uniquely determined by the homogeneous Helmholtz equation (6). The following lemma extends [1], [15] to the case in which the source is present.

Lemma 1. *The power spectral density of any spatially-stationary $h(\mathbf{r}, \mathbf{s})$ must be in the form of*

$$S(k_x, k_y, k_z, \kappa_x, \kappa_y, \kappa_z) = A^2(k_x, k_y, k_z, \kappa_x, \kappa_y, \kappa_z) \delta(k_x^2 + k_y^2 + k_z^2 - \kappa^2) \delta(\kappa_x^2 + \kappa_y^2 + \kappa_z^2 - \kappa^2) \quad (58)$$

for $k_z, \kappa_z \geq 0$ and with $A(k_x, k_y, k_z, \kappa_x, \kappa_y, \kappa_z)$ being a real-valued non-negative function.

Proof. The proof is given in Appendix C and follows from the channel's reciprocity principle. \square

The above lemma specifies the form that the power spectral density $S(k_x, k_y, k_z, \kappa_x, \kappa_y, \kappa_z)$ of a spatially-stationary channel must always have. This is due to the statistical implication of

wave propagation on the second-order statistics of the spatial random field $h(\mathbf{r}, \mathbf{s})$. Particularly, Lemma 1 states that $S(k_x, k_y, k_z, \kappa_x, \kappa_y, \kappa_z)$ must vanish everywhere except on the spectral support given by a pair of centered, upper-hemispheres $\mathcal{S}_+ \times \mathcal{S}_+$ of radius κ , as illustrated in Fig. 6. At the source, e.g., \mathcal{S}_+ is defined as

$$\mathcal{S}_+ = \{(\kappa_x, \kappa_y, \kappa_z) \in \mathbb{R}^3 : \kappa_x^2 + \kappa_y^2 + \kappa_z^2 = \kappa^2, \kappa_z \geq 0\}. \quad (59)$$

The term $A^2(k_x, k_y, k_z, \kappa_x, \kappa_y, \kappa_z)$ in (58) describes how the channel power is distributed over the spectral support $\mathcal{S}_+ \times \mathcal{S}_+$. We refer to it as *spectral factor*. The simplest model is obtained by requiring the spectral factor to be separable and uniform on every source and receive propagation direction. This simplification leads to an *isotropic channel* [48]. In this case, the normalized spectral factor in (58), for a channel with unit average power, is given by $A^2(k_x, k_y, k_z, \kappa_x, \kappa_y, \kappa_z) = A^2(\kappa)$ for $(\kappa_x, \kappa_y, \kappa_z) \in \mathcal{S}_+$ and $(k_x, k_y, k_z) \in \mathcal{S}_+$ with [15]

$$A^2(\kappa) = 2\pi^2/\kappa. \quad (60)$$

The isotropic model will be discussed in more details in Section V and Section VII. We stress that isotropy is a particular instance of our model, which remains valid for any arbitrary spectral factor $A^2(k_x, k_y, k_z, \kappa_x, \kappa_y, \kappa_z)$.

In Appendix C, it is shown that $S(k_x, k_y, \kappa_x, \kappa_y)$ in (56) is related to $S(k_x, k_y, k_z, \kappa_x, \kappa_y, \kappa_z)$ in (58) through

$$S(k_x, k_y, \kappa_x, \kappa_y) = \frac{1}{(2\pi)^2} e^{i(\gamma(\kappa_x, \kappa_y)s_z - \gamma(k_x, k_y)r_z)} \iint_{-\infty}^{\infty} S(k_x, k_y, k_z, \kappa_x, \kappa_y, \kappa_z) e^{i(k_z r_z - \kappa_z s_z)} dk_z d\kappa_z. \quad (61)$$

Hence, it is obtained by computing the spatial Fourier inversion of $S(k_x, k_y, k_z, \kappa_x, \kappa_y, \kappa_z)$ with respect to the free variables $k_z, \kappa_z \geq 0$ and by compensating for the phase shifts due to the migration filters. The structure of $S(k_x, k_y, \kappa_x, \kappa_y)$ in (56) is determined by this transformation, which is further discussed next.

D. Average channel power

The average channel power $P_h = \mathbb{E}\{|h(\mathbf{r}, \mathbf{s})|^2\}$ is obtained by integrating the power spectral density $S(k_x, k_y, k_z, \kappa_x, \kappa_y, \kappa_z)$ in (58) over its entire support. Notice that it does not depend on the distance between the source and receive locations as a direct consequence of the stationarity

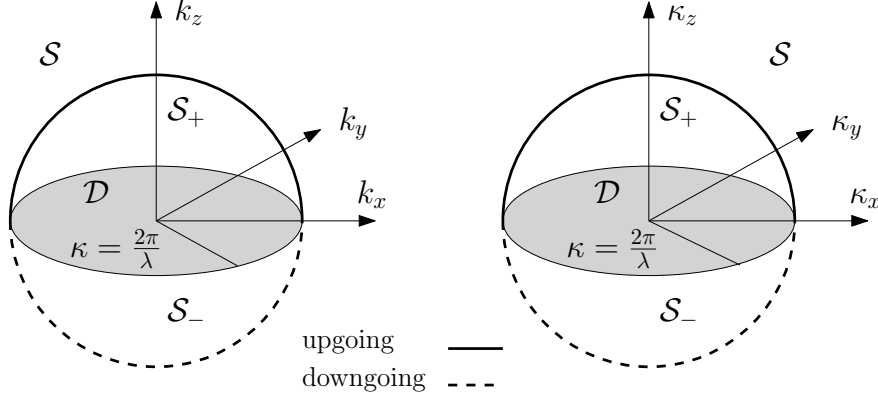


Fig. 6. The power spectral density $S(k_x, k_y, k_z, \kappa_x, \kappa_y, \kappa_z)$ of a spatially-stationary channel $h(\mathbf{r}, \mathbf{s})$ is given by Lemma 1 and is defined on the impulsive set $\mathcal{S}_+ \times \mathcal{S}_+$ with \mathcal{S}_+ given by (59). When \mathcal{S}_+ is parametrized onto a 2D disk \mathcal{D} we obtain $S(k_x, k_y, \kappa_x, \kappa_y)$ in (61) defined on $\mathcal{D} \times \mathcal{D}$.

assumption, which physically hides the action-at-distance effect due to wave propagation into a lossy medium. We can equivalently compute P_h by using (55). Since $P_h = c_h(\mathbf{0}, \mathbf{0})$, we obtain

$$P_h = \frac{1}{(2\pi)^4} \iiint_{-\infty}^{\infty} S(k_x, k_y, \kappa_x, \kappa_y) d\kappa_x d\kappa_y dk_x dk_y \quad (62)$$

$$\stackrel{(a)}{=} \frac{(\kappa\eta)^2}{2(2\pi)^4} \iiint_{-\infty}^{\infty} \frac{A^2(k_x, k_y, \kappa_x, \kappa_y)}{\gamma(k_x, k_y)\gamma(\kappa_x, \kappa_y)} d\kappa_x d\kappa_y dk_x dk_y \quad (63)$$

where (a) follows from (56). In light of (62), $S(k_x, k_y, \kappa_x, \kappa_y)$ can be regarded as the 4D power spectral density of $h(\mathbf{r}, \mathbf{s})$. If we assume that $h(\mathbf{r}, \mathbf{s})$ has unit average power, then the integration in (62) over the entire support must yield 1. In this case, $S(k_x, k_y, \kappa_x, \kappa_y)$ represents the *continuous angular power distribution* of the channel, which specifies how the power is distributed angularly between every pair of source $\hat{\mathbf{k}}$ and receive $\hat{\mathbf{k}}$ propagation directions, on average.

As observed in [15], the integration in (61) is equivalent to parametrizing each 3D spectral upper-hemisphere \mathcal{S}_+ in (59) onto the 2D spectral disk \mathcal{D} in (19); see Fig. 6. Therefore, $A^2(k_x, k_y, \kappa_x, \kappa_y)$ in (56) describes how the channel power is distributed over the spectral support $\mathcal{D} \times \mathcal{D}$, i.e., it represents the average angular power transfer between the source $\hat{\mathbf{k}}$ and receive $\hat{\mathbf{k}}$ propagation directions.⁷ Notice that $A(k_x, k_y, \kappa_x, \kappa_y)$ is related to the 6D spectral factor $A(k_x, k_y, k_z, \kappa_x, \kappa_y, \kappa_z)$ through (141), that is, is obtained by sampling the spectral hemispheres

⁷We recall that the longitudinal coordinates (κ_z, k_z) of $\hat{\mathbf{k}}$ and $\hat{\mathbf{k}}$ are parametrized by the other coordinates (κ_x, κ_y) and (k_x, k_y) , respectively.

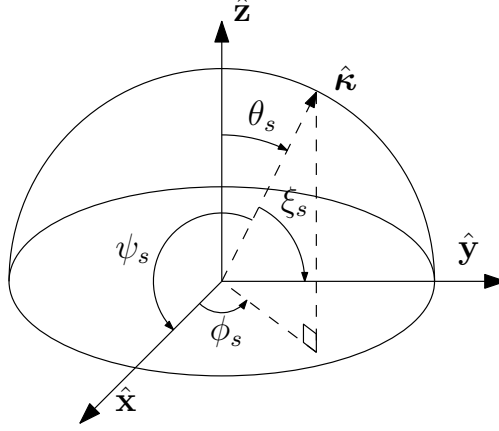


Fig. 7. Cosine directions and spherical coordinates defined on the unit upper-hemisphere.

$\mathcal{S}_+ \times \mathcal{S}_+$ angularly, and then, rescaling. Also, in (56) the terms $\gamma(k_x, k_y)$ and $\gamma(\kappa_x, \kappa_y)$, as defined in (22), are the Jacobians of the plane-wave parametrization of \mathcal{S}_+ onto its 2D lower dimensional counterpart \mathcal{D} .

V. PHYSICAL MODELING OF THE SPECTRAL FACTOR

We now show how the spectral factor $A(k_x, k_y, \kappa_x, \kappa_y)$ can be modelled to account for a realistic propagation scenario. To do so, in Appendix D we change the domain of representation from cosine directions to spherical coordinates (i.e., elevation and azimuth), as illustrated in Fig. 7, e.g., at the source. Representing the spectral factor in spherical coordinates is more convenient for two reasons: engineers are used to work with spherical angles rather than cosine directions, and the terms $\gamma(k_x, k_y)$ and $\gamma(\kappa_x, \kappa_y)$ at the denominator of (63) disappear after the transformation as they are embedded into the Jacobian of this map. In particular, by using (149) into (63) and embedding all constants into the spectral factor we obtain

$$P_h = \iiint_{\mathcal{S}_+ \times \mathcal{S}_+} A^2(\theta_r, \phi_r, \theta_s, \phi_s) d\Omega_s d\Omega_r \quad (64)$$

where $d\Omega_r = \sin \theta_r d\theta_r d\phi_r$ and $d\Omega_s = \sin \theta_s d\theta_s d\phi_s$ are respectively the differential elements of solid angles pointed by $\hat{\kappa}$ and $\hat{\mathbf{k}}$, which are defined over the unit upper-hemisphere \mathcal{S}_+ in (145). Compared to (62), (64) describes the average angular power transfer in spherical coordinates. Under the same unit average power constraint, i.e., $P_h = 1$, $A^2(\theta_r, \phi_r, \theta_s, \phi_s)$ represents the continuous angular power distribution of the channel specifying the power transfer between every

pair of source (θ_s, ϕ_s) and receive (θ_r, ϕ_r) directions, i.e., $A^2(\theta_r, \phi_r, \theta_s, \phi_s) = p_{A^2}(\theta_r, \phi_r, \theta_s, \phi_s)$ that is such that

$$\iiint_{\mathcal{S}_+ \times \mathcal{S}_+} p_{A^2}(\theta_r, \phi_r, \theta_s, \phi_s) d\Omega_s d\Omega_r = 1. \quad (65)$$

The spectral characteristics of $h(\mathbf{r}, \mathbf{s})$ thus depend on the angular distribution $p_{A^2}(\theta_r, \phi_r, \theta_s, \phi_s)$ that physically accounts for the angular selectivity of the scattering.

A. Discrete scattering

Both indoor and outdoor wireless measurement campaigns [49]–[51] have shown that the transfer of power is typically *clustered* about some $N_c \geq 1$ modal propagation directions at source and receiver. Hence, a physically meaningful and intuitive characterization of the channel angularly is obtained by assuming the radiated power to be coupled in the neighbourhood of these N_c modal directions, which are also called as *rays* or *paths* [9], [56]. In particular, let \mathcal{C}_i be a set of propagation directions connecting the source and receiver within the i -th cluster with $i = 1, \dots, N_c$. The resulting angular distribution $p_{A^2}(\theta_r, \phi_r, \theta_s, \phi_s)$ is then discrete and given by

$$p_{A^2}(\theta_r, \phi_r, \theta_s, \phi_s) = \sum_{i=1}^{N_c} \sum_{j \in \mathcal{C}_i} \Gamma_j \delta(\hat{\boldsymbol{\kappa}}(\theta_s, \phi_s) - \hat{\boldsymbol{\kappa}}_j) \delta(\hat{\mathbf{k}}(\theta_r, \phi_r) - \hat{\mathbf{k}}_j) \quad (66)$$

where Γ_j is the (normalized) complex propagation coefficient that turns every incident plane-wave $a_s(\boldsymbol{\kappa}_j, \mathbf{s})$ to direction $\hat{\boldsymbol{\kappa}}_j = \hat{\boldsymbol{\kappa}}(\theta_{s,j}, \phi_{s,j})$ into another received plane-wave $a_r(\mathbf{k}_j, \mathbf{r})$ from direction $\hat{\mathbf{k}}_j = \hat{\mathbf{k}}(\theta_{r,j}, \phi_{r,j})$ with $j \in \mathcal{C}_i$. The above expression describes a ray tracing model, which can be derived as a particular instance of our model by choosing an angular distribution of the form in (66). The generalization of (66) to a continuum of scatterers is discussed next.

B. Continuous scattering

We illustrate a few simple, but insightful, examples to model $p_{A^2}(\theta_r, \phi_r, \theta_s, \phi_s)$ that account for some specific propagation conditions.

1) *Isotropic distribution*: The simplest choice to model the angular distribution is as a bounded constant function, i.e., $p_{A^2}(\theta_r, \phi_r, \theta_s, \phi_s) = 1$, over its entire support $(\theta_r, \phi_r, \theta_s, \phi_s) \in \mathcal{S}_+ \times \mathcal{S}_+$ where \mathcal{S}_+ is the unit upper hemisphere in (145). This choice leads to a propagation scenario where the angular power transfer between source and receiver is distributed uniformly; that is, an isotropic channel. A direct consequence of having an isotropic scattering condition is that the angular distribution naturally decouples leading to a *separable* channel model.

2) *Piecewise-constant distribution*: A more realistic model that capture the angular selectivity of the underlying scattering mechanism is obtained by assuming the channel power to be clustered around some modal propagation directions and distributed uniformly within each cluster angular region [11, Sec. II]. Mathematically, $p_{A^2}(\theta_r, \phi_r, \theta_s, \phi_s)$ is chosen as a bounded piecewise constant function over non-overlapped angular sets, i.e., [11, Eq. (10)]

$$p_{A^2}(\theta_r, \phi_r, \theta_s, \phi_s) = \mathbb{1}_{\Theta_r}(\theta_r, \phi_r) \mathbb{1}_{\Theta_s}(\theta_s, \phi_s) \quad (67)$$

where $\Theta_r, \Theta_s \subseteq \mathcal{S}_+$ are the union of all angular regions $(\theta_r, \phi_r) \in \Theta_{r,i}$ and $(\theta_s, \phi_s) \in \Theta_{s,i}$ subtended by the i -th cluster for $i = 1, \dots, N_c$ and that are viewed from V_S and V_R , respectively.

3) *Separable distribution*: A generalized version of the model in (67) is obtained as

$$p_{A^2}(\theta_r, \phi_r, \theta_s, \phi_s) = p_{A_r^2}(\theta_r, \phi_r) p_{A_s^2}(\theta_s, \phi_s) \quad (68)$$

where $p_{A_s^2}(\theta_s, \phi_s)$ and $p_{A_r^2}(\theta_r, \phi_r)$ are two arbitrarily chosen angular distributions. These are responsible for modeling the angular selectivity separately at source and receiver, respectively. In the particular case where $p_{A_r^2}(\theta_r, \phi_r) = p_{A_s^2}(\theta_s, \phi_s)$, the channel is called *symmetric*. The model in (68) leads to a separable channel model in its most general form, also known as Kronecker model [52].

Next, we show how tools borrowed from directional statistics (e.g., [53]) can be successfully applied to model $p_{A^2}(\theta_r, \phi_r, \theta_s, \phi_s)$. To bring out the physical properties of our model, we still retain the separability assumption in (68) and focus on the angular distribution $p_{A_s^2}(\theta_s, \phi_s)$ at the source, as $p_{A_r^2}(\theta_r, \phi_r)$ at the receiver follows similarly. We drop the subscript s for convenience. In particular, by using the separability assumption in (68) into (65), and substituting $d\Omega = \sin(\theta)d\theta d\phi$, we obtain $\iint_{\mathcal{S}_+} p(\theta, \phi) \sin(\theta) d\theta = 1$. We notice that a coupled model can be treated alike but requires to tradeoff mathematical tractability—due to the higher number of parameters involved—with model accuracy.

C. 3D von Mises-Fisher distribution

We model each angular cluster $(\theta, \phi) \in \Theta_i$ independently as $p_i(\theta, \phi)$ with $i = 1, \dots, N_c$. The total angular density function $p(\theta, \phi)$, comprehensive of all clusters, is finally obtained as a weighted linear combination of all cluster contributions $\{p_i(\theta, \phi)\}$, i.e., the mixture

$$p(\theta, \phi) = \sum_{i=1}^{N_c} w_i p_i(\theta, \phi) \quad (69)$$

with weights $w_i \geq 0$ such that $\sum_{i=1}^{N_c} w_i = 1$. To model the i -th cluster, instead of choosing a particular distribution, we specify a family of distributions that is indexed by some parameters. This will enable us to model as many cases of interest as possible. A convenient family of angular distributions is the 3D von Mises-Fisher (vMF) family, which is defined on the unit upper-hemisphere \mathcal{S}_+ in (145) as [53, Eq. (9.3.4)]

$$p_i(\theta, \phi) = c(\alpha_i) e^{\alpha_i \hat{\boldsymbol{\mu}}_i^T \hat{\boldsymbol{\kappa}}(\theta, \phi)}, \quad \hat{\boldsymbol{\kappa}} \in \mathcal{S}_+ \quad (70)$$

where $c(\alpha_i) = \alpha_i / (4\pi \sinh(\alpha_i))$ is the normalization constant.⁸ A distribution of this sort is specified by the lowest number of parameters, i.e., a modal direction $\hat{\boldsymbol{\mu}}_i \in \mathcal{S}_+$ given by

$$\hat{\boldsymbol{\mu}}_i = \begin{pmatrix} \sin(\theta_{\mu,i}) \cos(\phi_{\mu,i}) \\ \sin(\theta_{\mu,i}) \sin(\phi_{\mu,i}) \\ \cos(\theta_{\mu,i}) \end{pmatrix} \quad (71)$$

and an angular concentration $\alpha_i \in [0, \infty)$. The former specifies the propagation direction around which the power is concentrated (i.e., elevation $\theta_{\mu,i}$ and azimuth $\phi_{\mu,i}$ angles of the modal direction) while the latter determines the angular concentration of $p_i(\theta, \phi)$, that is, as α_i increases the density becomes more and more concentrated around $\hat{\boldsymbol{\mu}}_i$. Notice that (70) can be rewritten in terms of spherical angles as

$$p_i(\theta, \phi) = c(\alpha_i) e^{\alpha_i (\sin(\theta) \sin(\theta_{\mu,i}) \cos(\phi - \phi_{\mu,i}) + \cos(\theta) \cos(\theta_{\mu,i}))}, \quad (\theta, \phi) \in \mathcal{S}_+ \quad (72)$$

where we expanded the inner product at the exponent while using (71) and (144). The total angular distribution $p(\theta, \phi)$ in (69) is therefore obtained as a mixture of 3D vMF distributions in (70), also referred to as $\hat{\boldsymbol{\kappa}} \sim M_3(\hat{\boldsymbol{\mu}}, \alpha)$, which is completely specified by its vector parameters $\hat{\mathbf{M}} = [\hat{\boldsymbol{\mu}}_1, \dots, \hat{\boldsymbol{\mu}}_{N_c}]$ and $\boldsymbol{\alpha} = [\alpha_1, \dots, \alpha_{N_c}]^T$.

The family of 3D vMF distributions has an important physical significance as discussed next. Henceforth, we drop the subscript i for convenience. For any $\alpha > 0$, $p(\theta, \phi)$ is unimodal and rotationally-symmetric about its modal direction $\hat{\boldsymbol{\mu}}$. As limiting cases [55], if $\alpha = 0$ then (70) reduces to an isotropic density function on \mathcal{S}_+ , i.e.,

$$p(\theta, \phi) = 1/4\pi, \quad \hat{\boldsymbol{\kappa}} \in \mathcal{S}_+ \quad (73)$$

⁸The classical vMF family of density functions is defined on a unit sphere [53]. Instead, we consider only the upper-half of the spherical support and divide the normalization constant by a factor of 2. This is possible since transfer of power in practical scenarios spans a very narrow angular interval in elevation [51].

which models an isotropic scattering scenario wherein power is distributed uniformly over every directions. This is the analog in spherical coordinates to the spectral factor's formula provided in (60) in cosine direction coordinates. On the contrary, if $\alpha = \infty$ then (70) becomes an impulsive function of the form

$$p(\theta, \phi) = \delta(\hat{\boldsymbol{\kappa}}(\theta, \phi) - \hat{\boldsymbol{\mu}}), \quad \hat{\boldsymbol{\kappa}} \in \mathcal{S}_+ \quad (74)$$

which models an unspredded propagation scenario with power concentrated in only one direction $\hat{\boldsymbol{\mu}}$. Like any other distribution, for the family of 3D vMF distributions we can define a mean value and covariance matrix $\mathbf{C}_{\hat{\boldsymbol{\kappa}}} = \mathbb{E}\{\hat{\boldsymbol{\kappa}}\hat{\boldsymbol{\kappa}}^T\}$. These are expressed as a function of $t = \hat{\boldsymbol{\mu}}^T \hat{\boldsymbol{\kappa}} \in [0, 1]$ respectively as $\mathbb{E}\{\hat{\boldsymbol{\kappa}}\} = \mathbb{E}\{t\}\hat{\boldsymbol{\mu}}_s$ and

$$\mathbf{C}_{\hat{\boldsymbol{\kappa}}} = \text{var}\{t\}\hat{\boldsymbol{\mu}}\hat{\boldsymbol{\mu}}^T + \frac{1 - \mathbb{E}\{t^2\}}{2}(\mathbf{I}_3 - \hat{\boldsymbol{\mu}}\hat{\boldsymbol{\mu}}^T). \quad (75)$$

For any vector $\hat{\boldsymbol{\mu}}$, the *circular variance* $\nu^2 = \text{tr}(\mathbf{C}_{\hat{\boldsymbol{\kappa}}})$ of $\hat{\boldsymbol{\kappa}}$ reads as

$$\nu^2 = 1 - (\mathbb{E}\{t\})^2 \in [0, 1] \quad (76)$$

where $\mathbb{E}\{t\}$ for the density function in (70) is given by [53, Eq. (9.3.9)]

$$\mathbb{E}\{t\} = \coth(\alpha) - 1/\alpha. \quad (77)$$

The limiting cases $\nu^2 = 1$ and $\nu^2 = 0$ correspond to the isotropic and impulsive angular density functions described in (73) and (74), respectively. Fig. 8 graphically illustrates the normalized distribution $p(\theta, \phi) \sin(\theta)$ where $p(\theta, \phi)$ is modeled using the mixture of 3D vMF distributions $\hat{\boldsymbol{\kappa}} \sim M_3(\hat{\mathbf{M}}, \alpha)$ described by (69) and (70) for different propagation environments, which correspond to different choices of the parameters $\hat{\mathbf{M}}$ and α . Notice that the determination of the parameter α from the circular variance ν^2 requires to solve the fixed-point equation obtained by substituting (77) into (76). An isotropic propagation is illustrated in Fig. 8b, i.e., with $\nu^2 = 1$, regardless of θ_μ and ϕ_μ . Angular selectivity is considered in Fig. 8a and Fig. 8c where the angular distribution with non-isotropic propagation is illustrated. In Fig. 8a, a propagation environment with a single cluster, i.e., $N_c = 1$, is considered with $\theta_\mu = 45^\circ$ and $\phi_\mu = 0^\circ$ and α is such that the circular variance is $\nu^2 = 0.01$. A mixture of $N_c = 3$ 3D vMF distributions with uniform weights $w_i = 1/N_c$ for $i = 1, 2, 3$ is illustrated in Fig. 8c with parameters $(\theta_{\mu,1}, \phi_{\mu,1}) = [45^\circ, 0^\circ]$, $(\theta_{\mu,2}, \phi_{\mu,2}) = [50^\circ, 90^\circ]$, $(\theta_{\mu,3}, \phi_{\mu,3}) = [20^\circ, 130^\circ]$, and circular variances $\nu_1^2 = 0.01$, $\nu_2^2 = 0.02$, and $\nu_3^2 = 0.004$.

As a final remark, notice that the developed angular model does not require the angular distribution $p(\theta_r, \phi_r, \theta_s, \phi_s)$ to be separable (and rotationally symmetric) as it is generally specified

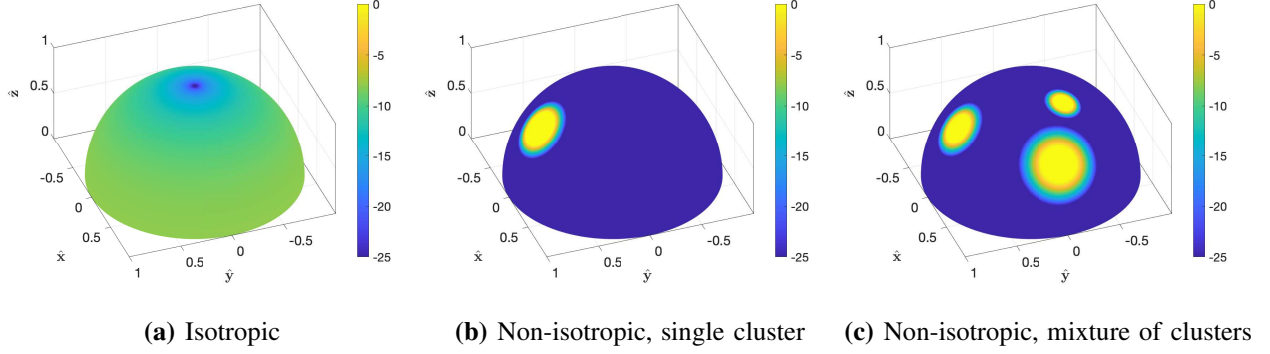


Fig. 8. Examples of the normalized 3D vMF angular distribution $p(\theta, \phi) \sin \theta$ in (70) for different propagation environments: isotropic, and non-isotropic with single and mixture of clusters.

by (65). This assumption has been used only to simplify the analysis. Notice that the 3D vMF distributions in (70) is directly obtained from a standard Gaussian distribution $\mathbf{k} \sim \mathcal{N}(\hat{\boldsymbol{\mu}}, \alpha^{-1}\mathbf{I})$ by applying the unit sphere constraint $\|\mathbf{k}\| = 1$, and then, rescaling [55]. Hence, like the 3D Gaussian distribution, the vMF distribution has circular contours of equal power centered on its modal direction $\hat{\boldsymbol{\mu}}$ [53]. A similar approach can be used to generate a more general angular distribution, e.g., with elliptical symmetry [54]. In general, a higher model accuracy can be achieved by introducing more parameters into the model, with an ensuing loss of analytical tractability.

VI. FOURIER SPECTRAL REPRESENTATION

We start by briefly recalling the Fourier spectral representation for a general time-domain, stationary random process and then will extend it to the case of interest, i.e., spatially-stationary random electromagnetic channel fields.

A. Time-domain stationary random processes

Signals can be represented as an integral superposition of complex harmonic oscillations via the classical inverse Fourier transform. Similarly, complex-Gaussian random processes may be represented as an integral superposition of statistically-independent complex harmonic oscillations. For a zero-mean, time-domain, stationary random process $\{h(t); t \in \mathbb{R}\}$ of finite bandwidth B that contains no periodic terms such representation is given by [43]

$$h(t) = \frac{1}{\sqrt{2\pi}} \int_{-\infty}^{\infty} H(\omega) e^{i\omega t} d\omega \quad (78)$$

where $H(\omega)$ plays exactly the same role as the Fourier transform of a finite energy signal and is given by

$$H(\omega) = S^{1/2}(\omega)W(\omega), \quad \omega \in \Omega \quad (79)$$

with $S(\omega)$ being an absolutely continuous power spectral density of $h(t)$ and $W(\omega)$ a complex white-noise random process with unit variance. The above spectral decomposition of $h(t)$ is known as *Fourier spectral representation* and accomplishes the same result for a stationary process $h_T(t)$, observed over the interval $t \in [0, T]$, as $BT \rightarrow \infty$ that the Karhunen-Loeve decomposition does for finite BT values. That is, it provides us with an orthonormal description of the channel with a continuum of statistically independent random Gaussian coefficients $H(\omega)$ with $\omega \in [-B, B]$. The mean-square convergence of (78) to the actual process is ensured by the Mercer's theorem [6], [43] for any random process with finite average power

$$P_h = \frac{1}{2\pi} \int_{-\infty}^{\infty} S(\omega) d\omega < \infty. \quad (80)$$

When a stationary random process $h(t)$ is truncated within the time interval $t \in [0, T]$, we observe another time-limited process $h_T(t)$. Every realization of $h(t)$ is multiplied by a unit energy rectangular window $w_T(t) = \mathbb{1}_{[0, T]}(t)/T$, i.e., $h_T(t) = h(t)w_T(t)$, and the corresponding spectrum $H_T(\omega)$ is given by the convolutional operator:

$$H_T(\omega) = \int_{-\infty}^{\infty} H(\beta)T \text{sinc}((\omega - \beta)T) d\beta. \quad (81)$$

It thus follows that constraining $h(t)$ within the time interval $t \in [0, T]$ breaks the statistical independence of the Gaussian coefficients $H(\omega)$ in (78). In the regime $BT \rightarrow \infty$, by normalizing the frequency ω , we have that

$$\lim_{BT \rightarrow \infty} \frac{1}{BT} \text{sinc}(\omega BT) = \delta(\omega). \quad (82)$$

The substitution of (82) into (81) provides the independence of the Gaussian coefficients $H_T(\omega)$ in the regime $BT \rightarrow \infty$, as expected. For large, but finite, BT values, the use of a Fourier series expansion of $h_T(t)$ is more appropriate as it can be regarded as an asymptotic Karhunen-Loeve decomposition that is valid for $BT \gg 1$ [43]. The transition between the two would be analogous to the classical Fourier series-Fourier integral transition for deterministic signals. Both representations coincide for $BT \rightarrow \infty$. However, to understand the fundamental limits of a time-domain communications system, integral representations of the form in (78) are easier to work with.

B. Spatially-stationary random electromagnetic channel

We have shown that the channel response $h(\mathbf{r}, \mathbf{s})$ between every two parallel z -planes at source and receiver can be modeled as a zero-mean, spatially-stationary, random field of finite bandwidth Ω given by (52). As shown in Section III-E, plane-waves observed over parallel z -planes coincides to phase-shifted version of 2D complex harmonic oscillations. In light of this, we seek a 4D Fourier spectral representation of $h(\mathbf{r}, \mathbf{s})$ that is parametrized by r_z and s_z . This follows directly from (41), by using (42) and the results in Theorem 2.

Lemma 2. *The 4D Fourier spectral representation of $h(\mathbf{r}, \mathbf{s})$ parametrized by r_z and s_z is given by (41) with*

$$H(k_x, k_y, \kappa_x, \kappa_y; r_z, s_z) = S^{1/2}(k_x, k_y, \kappa_x, \kappa_y) W(k_x, k_y, \kappa_x, \kappa_y) e^{i\gamma(k_x, k_y)r_z} e^{-i\gamma(\kappa_x, \kappa_y)s_z} \quad (83)$$

where $W(k_x, k_y, \kappa_x, \kappa_y)$ being a 4D circularly-symmetric, white-noise random field with unit variance and $S(k_x, k_y, \kappa_x, \kappa_y)$ is defined in (56).

Proof. The result easily follows by substituting the angular response (48) into (42). Then, Mercer's theorem [6], [43] provides the mean-square convergence of (41) with (83) for any $h(\mathbf{r}, \mathbf{s})$ with finite power P_h in (63). This condition is always satisfied by a bounded, piecewise continuous spectral factor $A(k_x, k_y, \kappa_x, \kappa_y)$ for which we can always find an arbitrary $A < \infty$ large enough such that

$$A(k_x, k_y, \kappa_x, \kappa_y) \leq A, \quad (k_x, k_y, \kappa_x, \kappa_y) \in \mathcal{D} \times \mathcal{D}. \quad (84)$$

The substitution of (84) into (62) yields

$$P_h \leq \left(\frac{\kappa\eta A/2}{(2\pi)^2} \iint_{\mathcal{D}} \frac{d\kappa_x d\kappa_y}{\gamma(\kappa_x, \kappa_y)} \right)^2 = \left(\frac{\kappa^2 \eta A}{8} \right)^2 < \infty \quad (85)$$

since $\iint_{\mathcal{D}} 1/\gamma(k_x, k_y) dk_x dk_y = \pi^2 \kappa$ as it follows from the radial symmetry of $\gamma(k_x, k_y)$ in (22). Notice that the condition (84) physically implies that the transfer of power between every transmit $\hat{\mathbf{k}}$ and receiver $\hat{\mathbf{k}}$ propagation directions is bounded across the entire angular domain. Hence, it is a reasonable condition that models every physical propagation environment of practical interest. \square

Comparing the 4D Fourier spectral representation of $h(\mathbf{r}, \mathbf{s})$ provided by Lemma 2 to its time domain counterpart in (78), we observe that the complex harmonic oscillations $e^{i\omega t}$ in (41) are replaced by the two 2D Fourier harmonics $\phi^*(\kappa_x, \kappa_y, s_x, s_y)$ and $\phi(k_x, k_y, r_x, r_y)$, and the

frequency response $H(\omega)$ by the 4D spectral response $H(k_x, k_y, \kappa_x, \kappa_y; r_z, s_z)$ in (83). We also notice that the phase-only dependance of $H(k_x, k_y, \kappa_x, \kappa_y; r_z, s_z)$ in (83) through the parameters r_z and s_z is due to the impulsive structure of the 6D power spectral density $S(k_x, k_y, k_z, \kappa_x, \kappa_y, \kappa_z)$ as reported in Lemma 1.

Suppose that V_S and V_R are two rectangular prisms of dimensions $\{L_{S,x}, L_{S,y}, L_{S,z}\}$ and $\{L_{R,x}, L_{R,y}, L_{R,z}\}$, respectively. Similarly to the time-domain case, the 4D Fourier spectral representation in Lemma 2 accomplishes the same result for the stationary field $h_V(\mathbf{r}, \mathbf{s})$ as $\min(\frac{L_{s,x}}{\lambda}, \frac{L_{s,y}}{\lambda}) \rightarrow \infty$ and $\min(\frac{L_{r,x}}{\lambda}, \frac{L_{r,y}}{\lambda}) \rightarrow \infty$ that the Karhunen-Loeve decomposition does for finite $(\frac{L_{s,x}}{\lambda}, \frac{L_{s,y}}{\lambda})$ and $(\frac{L_{r,x}}{\lambda}, \frac{L_{r,y}}{\lambda})$ values. That is, it provides us with an orthonormal description of the spatial channel, between every two parallel z -planes at source and receiver, with statistically independent Gaussian coefficients.

From (11), it follows that $h(\mathbf{r}, \mathbf{s})$ is in practice nonzero over the finite volumes V_R and V_S and only a truncated version $h_V(\mathbf{r}, \mathbf{s})$ of it is observed. For example, at the source every realization of $h(\mathbf{r}, \mathbf{s})$ is multiplied by a 2D unit energy rectangular window

$$w_{L_{S,x}L_{S,y}}(s_x, s_y) = \mathbb{1}_{[0, L_{S,x}]}(s_x) \mathbb{1}_{[0, L_{S,y}]}(s_y) \quad (86)$$

which yields $h_V(\mathbf{r}, \mathbf{s}) = h(\mathbf{r}, \mathbf{s})w_{L_{S,x}L_{S,y}}(s_x, s_y)$ and the corresponding spectrum $H_{L_{S,x}L_{S,y}}(s_x, s_y)$ is obtained by a convolutional operator similar to (81). The statistical independence of the Gaussian coefficients $H_{L_{S,x}L_{S,y}}(s_x, s_y)$ can thus be retained in the regime $\min(L_{s,x}/\lambda, L_{s,y}/\lambda) \rightarrow \infty$. For large, but finite, $L_{s,x}/\lambda$ and $L_{s,y}/\lambda$ values, the use of a Fourier plane-wave series expansion of $h_V(\mathbf{r}, \mathbf{s})$ over parallel z -planes at source and receiver is more appropriate [1], [15]. The resulting series expansion can be regarded as an asymptotic Karhunen-Loeve decomposition of a spatially-stationary random electromagnetic channel that is valid for $\min(L_{s,x}/\lambda, L_{s,y}/\lambda) \gg 1$ [2], [15], [46]. Some cautions must be taken when deriving the Fourier plane-wave series expansion [1], [15]. This is due to the impulsive nature of the power spectral density of random electromagnetic channels, as shown in Lemma 1. Both representations coincide in the regime $\min(L_{s,x}/\lambda, L_{s,y}/\lambda) \rightarrow \infty$.

VII. ELECTROMAGNETIC WAVE PROPAGATION PROBLEM: COMPLETE MODEL

In Section III, we developed a physics-based deterministic channel model that accounts for the presence of material objects separating the source V_S and receive V_R volumes (see Fig. 3). As seen, only upgoing plane-waves travelling towards the upper-hemisphere $+\hat{z}$ are considered

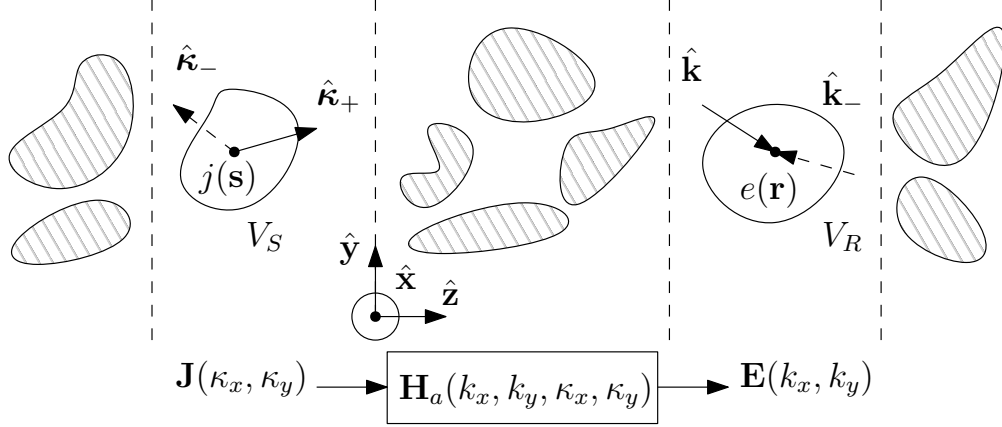


Fig. 9. Schematic diagram of wave propagation between two volumes V_S and V_R with material objects that may be spatially located everywhere in space. The electric current density $j(\mathbf{s})$ applied at V_S generates a vector-valued spectrum $\mathbf{J}(\kappa_x, \kappa_y) \in \mathbb{C}^2$ of incident plane-waves propagating towards directions $+\hat{\kappa}$ and $-\hat{\kappa}$. At the receiver, we observe another vector-valued spectrum $\mathbf{E}(k_x, k_y) \in \mathbb{C}^2$ of receive plane-waves impinging from directions $+\hat{\mathbf{k}}$ and $-\hat{\mathbf{k}}$. The scattering mechanism is fully embedded into an angular response matrix $\mathbf{H}_a(k_x, k_y, \kappa_x, \kappa_y) \in \mathbb{C}^{2 \times 2}$.

as they are solely responsible for the receive field $e(\mathbf{r})$. In other words, the LSV channel system operates under a causality condition. Starting from the physical model in Section III, we proposed in Section IV a second-order stochastic representation of the channel, which is built upon the spatial stationarity assumption.

In this section, we first extend the deterministic channel model to the general case where the material objects may be located everywhere in space (i.e., even in the left and right half-spaces of V_S and V_R , respectively). The complete wave propagation problem is illustrated in Fig. 9 and generalizes the propagation scenario depicted in Fig. 3 where material objects are confined entirely in a slab separating V_S and V_R . In general, the LSV channel system has causal (upgoing plane-waves) and anti-causal (downgoing plane-waves) parts due to wave propagation towards the upper- $+\hat{\mathbf{z}}$ and lower-hemispheres $-\hat{\mathbf{z}}$, respectively, both at source and receiver. Then, we show how the stochastic framework in Section IV can be applied to this generalized case.

A. Deterministic physical modeling

To distinguish between upgoing and downgoing plane-waves and fields we will use the subscripts $+$ and $-$, respectively. For example, the source and receive wave vectors associated to the upgoing plane-waves are $\boldsymbol{\kappa}_+$ and \mathbf{k}_+ as defined previously in Section III, whereas for downgoing plane-waves we have instead $\boldsymbol{\kappa}_- = \kappa_x \hat{\mathbf{x}} + \kappa_y \hat{\mathbf{y}} - \kappa_z \hat{\mathbf{z}}$ and $\mathbf{k}_- = k_x \hat{\mathbf{x}} + k_y \hat{\mathbf{y}} - k_z \hat{\mathbf{z}}$. With a slight abuse of notation, we will use $\boldsymbol{\kappa} = [\boldsymbol{\kappa}_+, \boldsymbol{\kappa}_-]^T$ and $\mathbf{k} = [\mathbf{k}_+, \mathbf{k}_-]^T$ throughout this section. The Weyl's identity (14) considering both the positive and negative parts of the spherical-wave solution (4) is

$$\frac{e^{i\kappa R}}{R} = \frac{i}{2\pi} \iint_{-\infty}^{\infty} \frac{e^{i(\kappa_x x + \kappa_y y + \kappa_z |z|)}}{\kappa_z} d\kappa_x d\kappa_y. \quad (87)$$

The 2D plane-wave representation of the incident field $e_i(\mathbf{r}')$ in (24) now reads as

$$e_i(\mathbf{r}') = \iint_{-\infty}^{\infty} d\kappa_x d\kappa_y \begin{cases} E_i^+(\kappa_x, \kappa_y) e^{i\boldsymbol{\kappa}_+^T \mathbf{r}'} & r'_z > \max_{V_S} s_z \\ E_i^-(\kappa_x, \kappa_y) e^{-i\boldsymbol{\kappa}_-^T \mathbf{r}'} & r'_z < \min_{V_S} s_z \end{cases} \quad (88)$$

where $E_i^\pm(\kappa_x, \kappa_y)$ are the complex amplitudes of the incident plane-waves propagating toward $\hat{\boldsymbol{\kappa}}_+$ and $\hat{\boldsymbol{\kappa}}_-$ given by

$$E_i^\pm(\kappa_x, \kappa_y) = \frac{1}{(2\pi)^2} \frac{\kappa\eta/2}{\kappa_z(\kappa_x, \kappa_y)} J^\pm(\kappa_x \kappa_y) \quad (89)$$

with

$$J^\pm(\kappa_x \kappa_y) = \int_{V_S} j(\mathbf{s}) e^{-i\boldsymbol{\kappa}_\pm^T \mathbf{s}} d\mathbf{s}. \quad (90)$$

Hence, the sole action of a volume source V_S is to create a vector-valued incident plane-wave spectrum $\mathbf{E}_i(\kappa_x, \kappa_y) = [E_i^+(\kappa_x, \kappa_y), E_i^-(\kappa_x, \kappa_y)]^T \in \mathbb{C}^2$ defined as

$$\mathbf{E}_i(\kappa_x, \kappa_y) = \frac{\kappa\eta/2}{(2\pi)^2 \kappa_z(\kappa_x, \kappa_y)} \mathbf{J}(\kappa_x \kappa_y) \quad (91)$$

where $\mathbf{J}(\kappa_x \kappa_y) = [J^+(\kappa_x \kappa_y), J^-(\kappa_x \kappa_y)]^T \in \mathbb{C}^2$ is given by

$$\mathbf{J}(\kappa_x \kappa_y) = \int_{V_S} j(\mathbf{s}) \mathbf{a}_s(\boldsymbol{\kappa}, \mathbf{s}) d\mathbf{s} \quad (92)$$

with $\mathbf{a}_s(\boldsymbol{\kappa}, \mathbf{s}) = [e^{-i\boldsymbol{\kappa}_+^T \mathbf{s}}, e^{-i\boldsymbol{\kappa}_-^T \mathbf{s}}]^T \in \mathbb{C}^2$ are the plane-waves corresponding to the two spectrums.

Upon interaction of the incident field $e_i(\mathbf{r}')$ with the material objects, a scattered received field $e(\mathbf{r})$ is created accordingly. Similarly to the incident field, this is composed of an upgoing and

a downgoing receive plane-waves impinging from $\hat{\mathbf{k}}_+$ and $\hat{\mathbf{k}}_-$, respectively. The total received field is described by a 2D plane-wave representation as in (31) of the form

$$\begin{aligned} e(\mathbf{r}) &= \iint_{-\infty}^{\infty} (E^+(k_x, k_y)e^{i\mathbf{k}_+^T \mathbf{r}} + E^-(k_x, k_y)e^{i\mathbf{k}_-^T \mathbf{r}}) dk_x dk_y \\ &= \iint_{-\infty}^{\infty} \mathbf{a}_r^T(\mathbf{k}, \mathbf{r}) \mathbf{E}(k_x, k_y) dk_x dk_y, \quad \mathbf{r} \in V_R \end{aligned} \quad (93)$$

where $\mathbf{E}(k_x, k_y) = [E^+(k_x, k_y), E^-(k_x, k_y)]^T \in \mathbb{C}^2$ is the vector-valued receive plane-wave spectrum with associated plane-waves $\mathbf{a}_r(\mathbf{k}, \mathbf{r}) = [e^{i\mathbf{k}_+^T \mathbf{r}}, e^{i\mathbf{k}_-^T \mathbf{r}}]^T \in \mathbb{C}^2$.

In brief, as sketched at the bottom of Fig. 9, there are two incident plane-wave spectrums in the form of a vector-valued incident spectrum $\mathbf{E}_i(\kappa_x, \kappa_y)$ that uniquely describe the upgoing and downgoing components of the incident field $e_i(\mathbf{r}')$. At the receiver, we measure a receive field $e(\mathbf{r})$ that is due to the contribution to the upgoing and downgoing components described by another vector-valued receive spectrum $\mathbf{E}(k_x, k_y)$. In general, there are four possible physical interactions among these spectrums and the entire linear scattering mechanism is completely described by a *scattering kernel matrix*

$$\mathbf{K}(k_x, k_y, \kappa_x, \kappa_y) = \begin{pmatrix} K^{++}(k_x, k_y, \kappa_x, \kappa_y) & K^{+-}(k_x, k_y, \kappa_x, \kappa_y) \\ K^{-+}(k_x, k_y, \kappa_x, \kappa_y) & K^{--}(k_x, k_y, \kappa_x, \kappa_y) \end{pmatrix} \in \mathbb{C}^{2 \times 2}. \quad (94)$$

The receive plane-wave spectrum $\mathbf{E}(k_x, k_y)$ is obtained as an integral superposition of all $\mathbf{E}_i(\kappa_x, \kappa_y)$ as

$$\mathbf{E}(k_x, k_y) = \iint_{-\infty}^{\infty} \mathbf{K}(k_x, k_y, \kappa_x, \kappa_y) \mathbf{E}_i(\kappa_x, \kappa_y) d\kappa_x d\kappa_y. \quad (95)$$

We notice that the scalar relationship $E(k_x, k_y) = (\mathbb{K}E_i)(k_x, k_y)$ in (33) can be obtained as a particular instance of (95) by setting to zero all entries of $\mathbf{K}(k_x, k_y, \kappa_x, \kappa_y)$ but the one associated to upgoing plane-waves only. As another example, by setting to zero the second column of $\mathbf{K}(k_x, k_y, \kappa_x, \kappa_y)$ we obtain the partial complete channel model at the receive side only provided in [15].

By substitution and electromagnetic reciprocity, a result analogous to Theorem 1 is obtained as summarized next.

Theorem 3. *The channel response $h(\mathbf{r}, \mathbf{s})$ of reciprocal propagation medium is generally given by the 4D Fourier plane-wave representation*

$$h(\mathbf{r}, \mathbf{s}) = \frac{1}{(2\pi)^2} \iiint_{-\infty}^{\infty} \mathbf{a}_r^T(\mathbf{k}, \mathbf{r}) \mathbf{H}_a(k_x, k_y, \kappa_x, \kappa_y) \mathbf{a}_s(\boldsymbol{\kappa}, \mathbf{s}) d\kappa_x d\kappa_y dk_x dk_y \quad (96)$$

with angular response matrix

$$\mathbf{H}_a(k_x, k_y, \kappa_x, \kappa_y) = \frac{\kappa\eta}{2} \frac{\mathbf{K}_a(k_x, k_y, \kappa_x, \kappa_y)}{k_z^{1/2}(k_x, k_y)\kappa_z^{1/2}(\kappa_x, \kappa_y)} \quad (97)$$

where $\mathbf{K}_a(\cdot)$ is a symmetric matrix with arbitrary complex-symmetric entries as defined in (123).

Proof. The proof is obtained by extending the one provided in Appendix A for Theorem 1 to vector-valued plane-wave spectrums. \square

Building on the analogy between plane-waves and 2D spatial-frequency Fourier harmonics, as discussed in Section III-E, the 4D Fourier representation in (41) of $h(\mathbf{r}, \mathbf{s})$ may still be used by introducing the spectral response

$$H(k_x, k_y, \kappa_x, \kappa_y; r_z, s_z) = [e^{ik_z(k_x, k_y)r_z}, e^{-ik_z(k_x, k_y)r_z}] \mathbf{H}_a(k_x, k_y, \kappa_x, \kappa_y) [e^{-i\kappa_z(\kappa_x, \kappa_y)s_z}, e^{i\kappa_z(\kappa_x, \kappa_y)s_z}]^T. \quad (98)$$

B. Statistical characterization

When the channel's fading is randomly space-variant the angular response matrix $\mathbf{H}_a(k_x, k_y, \kappa_x, \kappa_y)$ and, in turn, the channel response $h(\mathbf{r}, \mathbf{s})$, become random. A very desirable property for spatial random fields is stationarity under which a second-order characterization of $h(\mathbf{r}, \mathbf{s})$ was obtained in Theorem 2. If, in addition, we require $h(\mathbf{r}, \mathbf{s})$ to be a circularly-symmetric and complex-Gaussian spatial random field, this representation completely characterizes the channel statistically. To achieve this, the entries of $\mathbf{H}_a(k_x, k_y, \kappa_x, \kappa_y)$ must be (i) zero-mean, (ii) uncorrelated with each other, and individually having (iii) autocorrelation function proportional to a Dirac delta function and (iv) circularly-symmetric, complex-Gaussian distribution. The main result is summarized next.

Theorem 4. *If $h(\mathbf{r}, \mathbf{s})$ is a spatially-stationary, circularly-symmetric and complex-Gaussian random field, the angular response matrix $\mathbf{H}_a(k_x, k_y, \kappa_x, \kappa_y)$ in (96) must be of the form*

$$\frac{\kappa\eta}{2} \frac{\mathbf{A}(k_x, k_y, \kappa_x, \kappa_y) \odot \mathbf{W}(k_x, k_y, \kappa_x, \kappa_y)}{\gamma^{1/2}(k_x, k_y)\gamma^{1/2}(\kappa_x, \kappa_y)} \quad (99)$$

where $(k_x, k_y, \kappa_x, \kappa_y) \in \mathcal{D} \times \mathcal{D}$ with \mathcal{D} being the centered disk of radius κ given in (19). Here, $\mathbf{A}(k_x, k_y, \kappa_x, \kappa_y)$ is a real-valued, non-negative 2×2 matrix function and

$$\mathbf{W}(k_x, k_y, \kappa_x, \kappa_y) = \begin{pmatrix} W^{++}(k_x, k_y, \kappa_x, \kappa_y) & W^{+-}(k_x, k_y, \kappa_x, \kappa_y) \\ W^{-+}(k_x, k_y, \kappa_x, \kappa_y) & W^{--}(k_x, k_y, \kappa_x, \kappa_y) \end{pmatrix} \quad (100)$$

with i.i.d. entries $W^{\pm\pm}(k_x, k_y, \kappa_x, \kappa_y)$ distributed as

$$W^{\pm\pm}(k_x, k_y, \kappa_x, \kappa_y) \sim \mathcal{N}_{\mathbb{C}}(0, 1). \quad (101)$$

In view of the fact that wave propagation is still modeled by the same physical constitutive equations, the 6D power spectral density $S(k_x, k_y, k_z, \kappa_x, \kappa_y, \kappa_z)$ of any physically-meaningful channel $h(\mathbf{r}, \mathbf{s})$ must yet be impulsive of the form in (58). With respect to the power spectral density described in Lemma 1, the spectral support is now given by a pair of centered, spheres $\mathcal{S} \times \mathcal{S}$ of radius κ , as illustrated in Fig. 6. Each one of the two spectral spheres embeds the contributions due to the causal \mathcal{S}_+ and anti-causal \mathcal{S}_- part, i.e., $\mathcal{S} = \mathcal{S}_+ \cup \mathcal{S}_-$.

VIII. CONNECTIONS TO OTHER CHANNEL MODELS

As stated in the introduction, the provided spatial characterization of electromagnetic channels generalizes other well-known models already available in the research literature. This is discussed next in detail. For simplicity, we focus on the wave propagation problem described in Fig. 3.

A. Clarke's isotropic model and i.i.d. Rayleigh fading

As introduced earlier in Section IV and Section V, the isotropic channel constitutes the simplest propagation scenario [15]. This is obtained by requiring the spectral factor to be separable and uniform on every source and receive propagation directions with value given by (60). In the isotropic settings described above, the autocorrelation functions $c_h(\mathbf{r}, \mathbf{s})$ in (54) can be computed in closed-form and is given by $c_h(\mathbf{r}, \mathbf{s}) = c_{h,s}(\mathbf{s})c_{h,r}(\mathbf{r})$ with [15, Appendix III]

$$c_{h,r}(\mathbf{r}) = \text{sinc}\left(\frac{2R_r}{\lambda}\right) \quad (102)$$

where $R_r = \|\mathbf{r}\|$ is the distance among any pair of spatial points $(\mathbf{r}', \mathbf{r}' + \mathbf{r})$ at the receiver. A similar result holds for the $c_{h,s}(\mathbf{s})$ at the source. The above autocorrelation function coincides to the one obtained by using the Clarke's isotropic model [48]. In light of this, the developed channel model characterizes every spatially-stationary electromagnetic channels, while being in agreement with previous models.

The same key theoretical implications discussed in [15] for wave propagation at the receive side only can be extended to the more general case studied in this paper. In what follows we list the most interesting comments:

- The i.i.d. Rayleigh fading model [57] can only be used to model spatial samples of an isotropic channel wherein the antennas are deployed along a straight line at a spacing

of integer multiples of $\lambda/2$. In general, this model is strictly speaking incompatible with physics;

- The continuous-space wireless channel *always* exhibits spatial correlation. This is true even in the isotropic case where no angular selectivity is imposed by the scattering mechanism;
- The closest physically-tenable model to an i.i.d. Rayleigh fading model is the isotropic model. This is obtained as limiting case of an isotropic model by letting $\lambda \rightarrow 0$.

B. Deterministic far-field channel models

Elementary treatments of electromagnetic propagation (e.g., [8]) teach that the electric field generated by V_S can be represented by an incident plane-wave with planar wavefront at any point in the far-field region of the source, i.e., at a sufficient number of wavelengths from V_S . The electromagnetic far-field assumption is a cornerstone for the spatial characterization of electromagnetic channels available in the wireless communications literature, e.g., [9]–[11], [13]. Next, we briefly review its basic assumptions and implication on channel modeling.

Suppose that a point source is present at point \mathbf{s} and we wish to measure the electric field intensity $e(\mathbf{r}')$ generated at another point \mathbf{r}' . If the distance between two points \mathbf{s} and \mathbf{r}' is large enough compared to dimensions of the source volume V_S , we have the following *far-field* approximation (e.g. [11]):

$$1/\|\mathbf{r}' - \mathbf{s}\| \approx 1/\|\mathbf{r}'\|, \quad e^{i\kappa\|\mathbf{r}' - \mathbf{s}\|} \approx e^{i\kappa\|\mathbf{r}'\|} a_s(\boldsymbol{\kappa}, \mathbf{s}). \quad (103)$$

Here, $a_s(\boldsymbol{\kappa}, \mathbf{s}) = e^{-i\boldsymbol{\kappa}^T \mathbf{s}}$ is an incident plane-wave generated at point \mathbf{s} and propagating towards source direction $\hat{\boldsymbol{\kappa}} = \boldsymbol{\kappa}/\|\boldsymbol{\kappa}\|$, as defined in (27). By using (103) into the Green's function formula (4), the spherical-wave can be approximated as:

$$g(\mathbf{r}' - \mathbf{s}) \approx \frac{e^{i\kappa\|\mathbf{r}'\|}}{4\pi\|\mathbf{r}'\|} a_s(\boldsymbol{\kappa}, \mathbf{s}). \quad (104)$$

Hence, under the far-field electromagnetic assumption, spherical-waves generated by the source volume at every $\mathbf{s} \in V_S$ can be locally (in the neighbourhood of the point \mathbf{r}') approximated as plane-waves $a_s(\boldsymbol{\kappa}, \mathbf{s})$, all propagating towards the same direction $\hat{\boldsymbol{\kappa}}$. The wave propagation phenomena in the near- and far-field are illustrated in Fig. 2. By electromagnetic reciprocity, the same reasoning applies at the receiver for spherical-waves generated by the induced currents at every point on the material objects and measured at receive point \mathbf{r} .

C. 2D virtual channel model

There is a 2D counterpart to the 3D theory presented in this paper, where electromagnetic waves are generated by a line source [1]. Because of the cylindrical symmetry of the problem, wave propagation can be studied into a 2D infinite and homogeneous medium and $h(\mathbf{r}, \mathbf{s})$ depends on the horizontal Cartesian coordinates at source $\mathbf{s} = (s_z, s_y)$ and receive $\mathbf{r} = (r_z, r_y)$ locations. Any point source $-\delta(\mathbf{r}' - \mathbf{s})$ at $\mathbf{s} \in V_S$ generates a scalar cylindrical-wave that is described by the 2D Green's function

$$g(\mathbf{r}' - \mathbf{s}) = \frac{i}{4} H_0^{(1)}(\kappa \|\mathbf{r}' - \mathbf{s}\|). \quad (105)$$

The 2D counterpart of the Weyl's identity provides us with an exact representation of scalar cylindrical-waves as an integral superposition of plane-waves [8, Eq. (2.2.11)]

$$H_0^{(1)}(\kappa R) = \frac{1}{\pi} \int_{-\infty}^{\infty} \frac{e^{i(\kappa_x x + \kappa_y y)}}{\kappa_y} d\kappa_x \quad y > 0 \quad (106)$$

where $R = \sqrt{x^2 + y^2} > 0$ and

$$\kappa_y = \sqrt{\kappa^2 - \kappa_x^2} \in \mathbb{C} \quad (107)$$

that is determined by the other coordinate $\kappa_x \in \mathbb{R}$. By following the same procedure described in Section III, a 2D plane-wave representation of $h(\mathbf{r}, \mathbf{s})$ can be obtained similarly to the one provided in Theorem 1:

$$h(\mathbf{r}, \mathbf{s}) = \frac{1}{2\pi} \iint_{-\infty}^{\infty} a_r(\mathbf{k}, \mathbf{r}) H_a(k_x, \kappa_x) a_s(\boldsymbol{\kappa}, \mathbf{s}) d\kappa_x dk_x \quad (108)$$

where the angular response is given by

$$H_a(k_x, \kappa_x) = \frac{\kappa \eta}{2} \frac{K_a(k_x, \kappa_x)}{k_y^{1/2}(k_x) \kappa_y^{1/2}(\kappa_x)} \quad (109)$$

with $K_a(\cdot)$ being an arbitrary complex-symmetric kernel and $k_y(k_x)$ is defined similarly to (107).

Here, $H_a(k_x, \kappa_x)$ is sandwiched between the two array responses

$$a_r(\mathbf{k}, \mathbf{r}) = e^{i\mathbf{k}^T \mathbf{r}} = e^{i(k_x r_x + k_y(k_x) r_y)} \quad (110)$$

$$a_s(\boldsymbol{\kappa}, \mathbf{s}) = e^{i\boldsymbol{\kappa}^T \mathbf{s}} = e^{i(\kappa_x s_x + \kappa_y(\kappa_x) s_y)} \quad (111)$$

with $\boldsymbol{\kappa} = [\kappa_x, \kappa_y(\kappa_x)]^T$ and $\mathbf{k} = [k_x, k_y(k_x)]^T$ being the wave vectors at source and receiver, respectively.

When spatial stationarity is retained, the 4D power spectral density $S(k_x, k_y, \kappa_x, \kappa_y)$ of $h(\mathbf{r}, \mathbf{s})$ is defined on a double impulsive upper-semicircle of radius κ . Once parametrized over the spectral support

$$\mathcal{T} = \{(k_x, \kappa_x) \in \mathbb{R}^2 : |k_x| \leq \kappa, |\kappa_x| \leq \kappa\} \quad (112)$$

the 2D bandlimited spectrum $S(k_x, \kappa_x)$ fully describes the channel statistically. As a result, the angular response $H_a(k_x, \kappa_x)$ in (108) is modeled as zero-mean, circularly-symmetric and complex-Gaussian random field with autocorrelation proportional to a Dirac delta function in the angular domain

$$H_a(k_x, \kappa_x) = \frac{\kappa\eta}{2} \frac{A(k_x, \kappa_x)W(k_x, \kappa_x)}{\gamma^{1/2}(k_x)\gamma^{1/2}(\kappa_x)} \quad (113)$$

where $\gamma(\cdot)$ is the real part of κ_y in (107), $A(\cdot)$ is the nonnegative spectral factor with support $(k_x, \kappa_x) \in \mathcal{T}$, and $W(\cdot)$ is a complex white noise field with unit variance. The change of integration variable from cosine direction κ_x to polar coordinate is performed by the map $\mathcal{C} : \kappa_x/\kappa \rightarrow \theta_s$ where $\cos \theta_s = \kappa_x/\kappa$ so that $d\kappa_x = \kappa\gamma(\kappa_x)d\theta_s$. Here, $\gamma(\kappa_x) = \kappa \cos(\pi/2 - \theta_s) = \kappa \sin \theta_s$. The same may be done at the receiver with cosine direction k_x . Similarly to (65), by imposing a normalization condition on the channel's average power P_h , a 2D angular density function $p(\theta_r, \theta_s) = A^2(\theta_r, \theta_s)/P_h$ may be defined such that

$$\int_0^{\pi/2} \int_0^{\pi/2} p(\theta_r, \theta_s) d\theta_r d\theta_s = 1. \quad (114)$$

In polar coordinates, (108) yields the 2D Fourier plane-wave angular representation

$$h(\mathbf{r}, \mathbf{s}) = \frac{1}{2\pi} \int_0^{\pi/2} \int_0^{\pi/2} a_r(\theta_r, \mathbf{r}) H_a(\theta_r, \theta_s) a_s(\theta_s, \mathbf{s}) d\theta_r d\theta_s \quad (115)$$

where $H_a(\theta_r, \theta_s)$ is circularly-symmetric, complex-Gaussian and

$$a_r(\theta_r, \mathbf{r}) = e^{i\kappa(r_x \cos \theta_r + r_y \sin \theta_r)} \quad (116)$$

$$a_s(\theta_s, \mathbf{s}) = e^{-i\kappa(s_x \cos \theta_s + s_y \sin \theta_s)} \quad (117)$$

the 2D *virtual representation* of the channel [9], [10]. Unlike [9], [10], (115) is achieved without resorting to the far-field assumption (i.e., our model is also valid in the near-field) and is valid for any arbitrary volumes V_S and V_R .

As an application to the above 2D virtual representation, we recall the computation in [12] of the ergodic capacity for linear arrays. There, the 2D angular density function $p(\theta_r, \theta_s)$ in (114)

is chosen as bounded and piecewise constant with value $p_0 > 0$ over non-overlapped angular intervals subtended by the scattering clusters, i.e.,

$$p(\theta_r, \theta_s) = p_0, \quad (\theta_r, \theta_s) \in \cup_{i=1}^{N_c} \Theta_{r,i} \times \Theta_{s,i}. \quad (118)$$

Here, plane-waves that undergo multiple scatterings are attenuated most. This effect is included in the constant p_0 by adding a parameter that accounts for multiple scattering events that may occur in the propagation medium. We notice that the provided model in Section V extends the one used in [12] to arbitrary propagation environment.

IX. DISCUSSION AND OUTLOOK

The electromagnetic wave propagation problem into a general 3D scattered medium can always be modeled as a linear and space-variant system. A system of this sort is fully characterized by its channel response that can be exactly described in terms of plane-waves. This argument is supported by the fact that there is a deterministic closed-form analytical expression for the channel response that is valid irrespective of the distance between source and receiver. In the radiating near-field region – when reactive propagation mechanisms are excluded, due to the low-pass filter behavior of the channel – the channel becomes spatially-stationary. As for time-domain stationary Gaussian processes, we derived an integral Fourier spectral representation that provides an asymptotic second-order characterization of the channel in terms of statistically independent Gaussian random coefficients.

To bring out the key concept, in this paper we considered idealized antenna patterns and scalar (i.e., acoustic) electric fields. Non-idealities due to different antenna patterns may be added straightforwardly. In dealing with polarimetric antenna arrays, every antenna point is replaced by three mutually perpendicular electric dipoles [28]. Consequently, the electric field at every incident propagation direction $\hat{\mathbf{k}}$, e.g., at the source, becomes vector-valued. There are an horizontally polarized plane-wave and a vertically polarized plane-wave for each (κ_x, κ_y) with an associated 2×1 vector incident plane-wave spectrum. At the receiver, another 2×1 vector receive plane-wave spectrum for each (k_x, k_y) is observed. The developed plane-wave model can be updated accordingly [28], [58].

From an information-theoretic perspective, the developed model enables the design and analysis of spatial information-bearing systems [59]. There is a fundamental space-time duality between time and space information-bearing systems in which time is opportunely replaced by space [46].

In exploiting this duality, the same capacity-oriented analysis of time-domain random fading channels in [60] can be opportunely extended to space-domain random fading channels leading to integral expressions for the ergodic capacity.

When the source and receive arrays are of finite dimensions, only a finite number of plane-waves carries the essential channel information [15], [46]. This is analogous to the Nyquist-Shannon sampling theorem for band-limited waveform channels of bandwidth B and observed over a time interval of duration T where approximately $2BT$ samples carry the essential channel information. In this case, the Fourier plane-wave representation is replaced by a Fourier plane-wave series expansion, which is similar to the Fourier integral-Fourier series transition for time-domain signals [2], [15]. Suitably discretized in space, the Fourier plane-wave series expansion provides a powerful tool that can be used to statistically model propagation channels for the analysis and design of large antenna array technologies at arbitrary operating frequencies.

APPENDIX A

In this appendix we determine the structure of the angular response $H_a(k_x, k_y, \kappa_x, \kappa_y)$ in (37) such that the channel impulse response $h(\mathbf{r}, \mathbf{s})$ complies with the electromagnetic reciprocity theorem for a reciprocal medium. This theorem relates the mutual interactions between two electric sources $j(\mathbf{s})$ with $\mathbf{s} \in V_S$ and $j'(\mathbf{r})$ with $\mathbf{r} \in V_R$ and the corresponding transmitted fields $e(\mathbf{r})$ with $\mathbf{r} \in V_R$ and $e'(\mathbf{s})$ with $\mathbf{s} \in V_S$, respectively [8]. To this end, we define $h_V(\mathbf{r}, \mathbf{s})$ and $h'_V(\mathbf{s}, \mathbf{r})$ as the corresponding channel responses in these two cases, as respectively depicted in Fig. 10a and Fig. 10b. Each system is described by the convolutional model in (10). For a reciprocal medium, the following reciprocity relation exists [8, Eq. 1.3.23]

$$\int_{V_S} j(\mathbf{s}) e'(\mathbf{s}) d\mathbf{s} = \int_{V_R} j'(\mathbf{r}) e(\mathbf{r}) d\mathbf{r}. \quad (119)$$

If the two sources are identical everywhere in their corresponding volumes V_S and V_R , and the measurements and injection operations are carried out in a volume of same shape and size, i.e., $V_S = V_R = V$, the use of (10) into (119) implies that $h_V(\mathbf{r}, \mathbf{s}) = h'_V(\mathbf{s}, \mathbf{r})$. This equality, in turn, is satisfied by the unconstrained channel response due to (11) as

$$h(\mathbf{r}, \mathbf{s}) = h(\mathbf{s}, \mathbf{r}), \quad \mathbf{r} \in V, \mathbf{s} \in V. \quad (120)$$

In other words, based on the reciprocity theorem and the definition of the channel impulse response, $h(\mathbf{r}, \mathbf{s})$ must be insensitive to the interchange of source and receive locations.

We therefore interchange \mathbf{r} and \mathbf{s} in (41) to determine under what conditions on the angular response $H(k_x, k_y, \kappa_x, \kappa_y; r_z, s_z)$ the reciprocity relation (120) holds. After the change of integration variables $(k_x, k_y) = (-\kappa_x, -\kappa_y)$, and vice versa, we obtain

$$H(k_x, k_y, \kappa_x, \kappa_y; r_z, s_z) = H(-\kappa_x, -\kappa_y, -k_x, -k_y; s_z, r_z) \quad (121)$$

for $(k_x, k_y, \kappa_x, \kappa_y) \in \mathbb{R}^2 \times \mathbb{R}^2$. Since the spatial-frequency response can be decomposed as in (42), this symmetry relation applies to the angular response equivalently (upon change of orientation of the z -axis) as

$$H_a(k_x, k_y, \kappa_x, \kappa_y) = H_a(-\kappa_x, -\kappa_y, -k_x, -k_y) \quad (122)$$

for $(k_x, k_y, \kappa_x, \kappa_y) \in \mathbb{R}^2 \times \mathbb{R}^2$. Consequently, *reciprocity* in the spatial domain is equivalent to *symmetry* in the angular domain. This observation is instrumental to determine the structure of the angular response of the channel.

We notice from (36) that symmetry is never satisfied due to presence of the term $\kappa_z(\kappa_x, \kappa_y)$ at denominator, even for a symmetric scattering kernel $K(k_x, k_y, \kappa_x, \kappa_y)$. Let $K_a(k_x, k_y, \kappa_x, \kappa_y)$ be a complex-symmetric, arbitrary kernel, i.e.,

$$K_a(k_x, k_y, \kappa_x, \kappa_y) = K_a(-\kappa_x, -\kappa_y, -k_x, -k_y) \quad (123)$$

for $(k_x, k_y, \kappa_x, \kappa_y) \in \mathbb{R}^2 \times \mathbb{R}^2$. Without loss of generality, we rewrite the scattering kernel as

$$K(k_x, k_y, \kappa_x, \kappa_y) = K_a(k_x, k_y, \kappa_x, \kappa_y) \frac{\kappa_z^{1/2}(\kappa_x, \kappa_y)}{k_z^{1/2}(k_x, k_y)} \quad (124)$$

where $K_a(k_x, k_y, \kappa_x, \kappa_y)$ is defined in (123), and, similarly to (21), we define

$$\kappa_z^{1/2}(\kappa_x, \kappa_y) = \begin{cases} \gamma^{1/2}(\kappa_x, \kappa_y), & (\kappa_x, \kappa_y) \in \mathcal{D} \\ \frac{1+i}{\sqrt{2}} |\gamma(\kappa_x, \kappa_y)|^{1/2}, & (\kappa_x, \kappa_y) \in \mathcal{D}^c \end{cases} \quad (125)$$

with γ being defined in (22). Finally, the substitution of (124) into (36) yields

$$H_a(k_x, k_y, \kappa_x, \kappa_y) = \frac{\kappa\eta}{2} \frac{K_a(k_x, k_y, \kappa_x, \kappa_y)}{\kappa_z^{1/2}(k_x, k_y) \kappa_z^{1/2}(\kappa_x, \kappa_y)}. \quad (126)$$

Symmetry of the angular response directly follows from (126) and the angular symmetry of $\kappa_z(\kappa_x, \kappa_y)$ and $k_z(k_x, k_y)$ in (21). Notice that $K_a(k_x, k_y, \kappa_x, \kappa_y) = \delta(k_y - \kappa_y) \delta(k_x - \kappa_x)$ in the LoS case is equivalent to (34) in the integral sense.

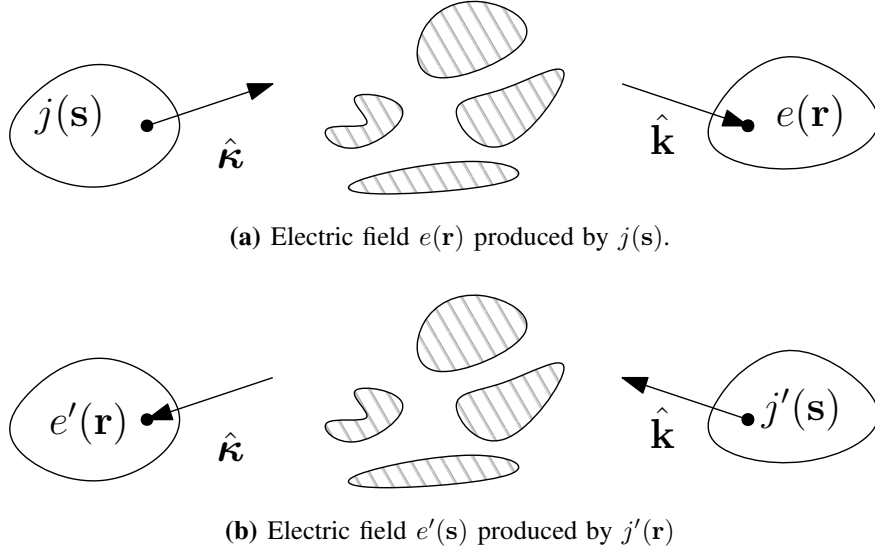


Fig. 10. Reciprocity relation for scalar electric sources.

APPENDIX B

Under stationarity, the average power of $h(\mathbf{r}, \mathbf{s})$ is required to be the same regardless of the pair $(\mathbf{r}_1, \mathbf{s}_1)$ and $(\mathbf{r}_2, \mathbf{s}_2)$ at which it is evaluated. Without loss of generality, let us assume $\mathbf{s}_1 = \mathbf{s}_2 = \mathbf{0}$ so that the average power depends on the receive point $\mathbf{r}_1 = \mathbf{r}_2$ only. We notice that the received plane-waves in (32) have different behavior depending on which region of their support is considered. Particularly, the substitution of $k_z(k_x, k_y)$ into (32) yields

$$a_r(\mathbf{k}, \mathbf{r}) = e^{i(k_x r_x + k_y r_y)} \begin{cases} e^{i\gamma(k_x, k_y)r_z}, & (k_x, k_y) \in \mathcal{D} \\ e^{-|\gamma(k_x, k_y)|r_z}, & (k_x, k_y) \in \overline{\mathcal{D}} \end{cases} \quad (127)$$

where γ is defined in (22). This relation implies that plane-waves with support $(k_x, k_y) \in \mathcal{D}$ have a real-valued κ_z and thus undergo a phase-shift when propagating towards any direction in the upper-hemisphere $\hat{\mathbf{z}}$. On the contrary, plane-waves having support $(k_x, k_y) \in \overline{\mathcal{D}}$ have an imaginary-valued κ_z and decay exponentially fast along z . Hence, we can split the integration domain of $h(\mathbf{r}, \mathbf{s})$ in (13) into two parts: $(\kappa_x, \kappa_y) \in \mathcal{D}$ and $(\kappa_x, \kappa_y) \in \overline{\mathcal{D}}$. The latter is responsible for the non-stationarity of $h(\mathbf{r}, \mathbf{0})$ and must be therefore excluded from our analysis. The same reasoning applied at the source leads to a necessary condition on $K_a(k_x, k_y, \kappa_x, \kappa_y)$ for $h(\mathbf{r}, \mathbf{s})$ in (2) to be spatially-stationary. In particular, $K_a(k_x, k_y, \kappa_x, \kappa_y)$ must vanishes in the evanescent region, i.e.,

$$K_a(k_x, k_y, \kappa_x, \kappa_y) \neq 0 \quad (\kappa_x, \kappa_y, k_x, k_y) \in \mathcal{D} \times \mathcal{D}. \quad (128)$$

In turn, by using (47) the above condition is equivalently satisfied by requiring

$$A(k_x, k_y, \kappa_x, \kappa_y) \neq 0 \quad (\kappa_x, \kappa_y, k_x, k_y) \in \mathcal{D} \times \mathcal{D}. \quad (129)$$

A sufficient condition on $K_a(k_x, k_y, \kappa_x, \kappa_y)$ for the stationarity of $h(\mathbf{r}, \mathbf{s})$ can be established by inspection of (2). In particular, the kernel $K_a(k_x, k_y, \kappa_x, \kappa_y)$ must be a collection of zero-mean and uncorrelated random variables, i.e.,

$$\mathbb{E}\{K_a(k_x, k_y, \kappa_x, \kappa_y)\} = 0 \quad (130)$$

$$\begin{aligned} \mathbb{E}\{K_a(k_x, k_y, \kappa_x, \kappa_y) K_a^*(k'_x, k'_y, \kappa'_x, \kappa'_y)\} &= A^2(k_x, k_y, \kappa_x, \kappa_y) \\ &\times \delta(k_x - k'_x) \delta(k_y - k'_y) \delta(\kappa_x - \kappa'_x) \delta(\kappa_y - \kappa'_y) \end{aligned} \quad (131)$$

where $A(\cdot)$ can be arbitrarily defined within the support $(k_x, k_y, \kappa_x, \kappa_y) \in \mathcal{D} \times \mathcal{D}$ due to (47). The above conditions (130) and (131) on the moments $K_a(k_x, k_y, \kappa_x, \kappa_y)$ can be summarized by requiring $W(k_x, k_y, \kappa_x, \kappa_y)$ to be a collection of unit-variance, independent and identically distributed (i.i.d.) circularly-symmetric and complex-Gaussian random variables, i.e.,

$$W(k_x, k_y, \kappa_x, \kappa_y) \sim \mathcal{N}_{\mathbb{C}}(0, 1). \quad (132)$$

The final expression for $H_a(k_x, k_y, \kappa_x, \kappa_y)$ is obtained by using (129) into (47) and reads as

$$H_a(k_x, k_y, \kappa_x, \kappa_y) = \frac{\kappa\eta}{2} \frac{A(k_x, k_y, \kappa_x, \kappa_y) W(k_x, k_y, \kappa_x, \kappa_y)}{\gamma^{1/2}(k_x, k_y) \gamma^{1/2}(\kappa_x, \kappa_y)} \quad (133)$$

where $W(k_x, k_y, \kappa_x, \kappa_y)$ is defined in (132). In (133), we substituted $k_z(k_x, k_y) = \gamma(k_x, k_y)$ and $\kappa_z(\kappa_x, \kappa_y) = \gamma(\kappa_x, \kappa_y)$ since we restricted (28) and (21) to the supports $(\kappa_x, \kappa_y) \in \mathcal{D}$ and $(k_x, k_y) \in \mathcal{D}$, at source and receiver, respectively.

APPENDIX C

By equating (55) and (57) and using the plane-wave formulas (27) and (32) we obtain

$$\frac{1}{(2\pi)^2} \iint_{-\infty}^{\infty} S(k_x, k_y, k_z, \kappa_x, \kappa_y, \kappa_z) e^{i(k_z r_z - \kappa_z s_z)} dk_z d\kappa_z \quad (134)$$

$$= S(k_x, k_y, \kappa_x, \kappa_y) e^{i(\gamma(k_x, k_y) r_z - \gamma(\kappa_x, \kappa_y) s_z)} \quad (135)$$

$$= (\kappa\eta)^2 A^2(k_x, k_y, \kappa_x, \kappa_y) \frac{e^{-i\gamma(\kappa_x, \kappa_y) s_z} e^{i\gamma(k_x, k_y) r_z}}{2\gamma(\kappa_x, \kappa_y) 2\gamma(k_x, k_y)} \quad (136)$$

where in the second equality we substituted the expression of $S(k_x, k_y, \kappa_x, \kappa_y)$ in (56) and $\gamma(\cdot)$ is defined in (22). As an intermediate step, notice that the composition of the Dirac delta function $\delta(x)$ with a differentiable function $g(x)$ yields

$$\delta(g(x)) = \sum_i \frac{\delta(x - x_i)}{|\frac{\partial g(x)}{\partial x}|_{x=x_i}}, \quad g(x_i) = 0, i = 1, 2, \dots \quad (137)$$

for a non-zero derivative $\partial g(x)/\partial x$. At the source side, e.g., by setting $g(\kappa_z) = \kappa_z^2 - \gamma^2(\kappa_x, \kappa_y)$ we have that

$$\delta(\kappa_z^2 - \gamma^2(\kappa_x, \kappa_y)) = \frac{\delta(\kappa_z - \gamma(\kappa_x, \kappa_y))}{2\gamma(\kappa_x, \kappa_y)}, \quad \kappa_z \geq 0 \quad (138)$$

where we only consider the positive solution associated to outgoing waves propagating towards $\hat{\mathbf{z}}$. Sampling of the Dirac delta function yields

$$\int_{-\infty}^{\infty} \delta(\kappa_z^2 - \gamma^2(\kappa_x, \kappa_y)) e^{-i\kappa_z s_z} d\kappa_z = \frac{e^{-i\gamma(\kappa_x, \kappa_y)s_z}}{2\gamma(\kappa_x, \kappa_y)}. \quad (139)$$

At the receive side, following the same procedure we obtain

$$\int_{-\infty}^{\infty} \delta(k_z^2 - \gamma^2(k_x, k_y)) e^{ik_z r_z} dk_z = \frac{e^{i\gamma(k_x, k_y)r_z}}{2\gamma(k_x, k_y)} \quad (140)$$

where we change the sign of the complex exponential and replace the transmit coordinates with the receive coordinates accordingly.

The power spectral density $S(k_x, k_y, k_z, \kappa_x, \kappa_y, \kappa_z)$ can be determined by inspection of (134) while using (139) and (140) into (136). The derived formula is finally reported in Lemma 1 where we introduced a 6D spectral factor $A(k_x, k_y, k_z, \kappa_x, \kappa_y, \kappa_z)$ that is related to $A(k_x, k_y, \kappa_x, \kappa_y)$ through

$$A(k_x, k_y, \kappa_x, \kappa_y) = \frac{A(k_x, k_y, \gamma(k_x, k_y), \kappa_x, \kappa_y, \gamma(\kappa_x, \kappa_y))}{2\pi\kappa\eta} \quad (141)$$

where $\gamma(\cdot)$ is defined in (22).

APPENDIX D

SPHERICAL COORDINATE REPRESENTATION OF THE SPECTRAL FACTOR

Consider the Cartesian wavenumber coordinates at the source, i.e., $(\kappa_x, \kappa_y, \gamma(\kappa_x, \kappa_y))$, which are parametrized by the horizontal coordinates (κ_x, κ_y) only. After normalizing with $\kappa = 2\pi/\lambda$, we obtain the normalized Cartesian coordinates $(\hat{\kappa}_x, \hat{\kappa}_y, \hat{\kappa}_z)$ of $\hat{\boldsymbol{\kappa}} = \hat{\kappa}_x \hat{\mathbf{x}} + \hat{\kappa}_y \hat{\mathbf{y}} + \hat{\kappa}_z \hat{\mathbf{z}}$ in (18) with $\hat{\kappa}_x = \kappa_x/\kappa$, $\hat{\kappa}_y = \kappa_y/\kappa$ and $\hat{\gamma}(\hat{\kappa}_x, \hat{\kappa}_y) = \gamma(\kappa_x, \kappa_y)/\kappa$ given by

$$\hat{\gamma}(\hat{\kappa}_x, \hat{\kappa}_y) = \sqrt{1 - \hat{\kappa}_x^2 - \hat{\kappa}_y^2} \quad (142)$$

where we used $\gamma(\cdot)$ as defined in (22). The triplet $(\hat{\kappa}_x, \hat{\kappa}_y, \hat{\gamma})$ is obtained by projecting the unit vector $\hat{\kappa}$ onto the Cartesian axes $(\hat{x}, \hat{y}, \hat{z})$, respectively. It thus follows that

$$(\hat{\kappa}_x, \hat{\kappa}_y, \hat{\gamma}) = (\cos(\psi_s), \cos(\xi_s), \cos(\theta_s)) \quad (143)$$

are the cosine of the angles between $\hat{\kappa}$ and the Cartesian axes $(\hat{x}, \hat{y}, \hat{z})$, as illustrated in Fig. 7. These are also referred to as *cosine directions* in physics (e.g., [30]). Conveniently, we can represent these cosine directions in terms of the spherical coordinates, i.e., elevation θ_s and azimuth ϕ_s angles (see Fig. 7), as

$$\begin{pmatrix} \hat{\kappa}_x \\ \hat{\kappa}_y \\ \hat{\gamma}(\hat{\kappa}_x, \hat{\kappa}_y) \end{pmatrix} = \begin{pmatrix} \sin(\theta_s) \cos(\phi_s) \\ \sin(\theta_s) \sin(\phi_s) \\ \cos(\theta_s) \end{pmatrix} \quad (144)$$

which are defined on the unit upper hemisphere

$$\mathcal{S}_+ = \{(\theta_s, \phi_s) : \theta_s \in [0, \pi/2], \phi_s \in [0, 2\pi)\}. \quad (145)$$

As expected, the cosine direction along \hat{z} can be derived from the other two by using $\hat{\kappa}_x$ and $\hat{\kappa}_y$ in (144) into (142) as $\hat{\gamma} = \sqrt{1 - \sin^2(\theta_s)} = \cos(\theta_s)$. As a consequence, the inverse map between the cosine directions and spherical coordinates is performed by $\mathcal{C} : (\hat{\kappa}_x, \hat{\kappa}_y) \rightarrow (\theta_s, \phi_s)$ that is readily obtained from (144) as

$$\theta_s = \sin^{-1} \left(\sqrt{\hat{\kappa}_x^2 + \hat{\kappa}_y^2} \right) \quad (146)$$

$$\phi_s = \tan^{-1} \left(\frac{\hat{\kappa}_y}{\hat{\kappa}_x} \right) \quad (147)$$

where the Jacobian of this map \mathcal{C} is given by

$$\left| \frac{\partial(\hat{\kappa}_x, \hat{\kappa}_y)}{\partial(\theta_s, \phi_s)} \right| = \cos(\theta_s) \sin(\theta_s). \quad (148)$$

It thus follows that the differentials of the two representations are related each other as

$$d\hat{\kappa}_x d\hat{\kappa}_y = \hat{\gamma}(\hat{\kappa}_x, \hat{\kappa}_y) \sin(\theta_s) d\theta_s d\phi_s \quad (149)$$

where we used $\hat{\gamma} = \cos(\theta_s)$ from (144). We finally notice that the same map $\mathcal{C} : (\hat{k}_x, \hat{k}_y) \rightarrow (\theta_r, \phi_r)$, applied here at the source, can also be used at the receiver to obtain a representation of the unit vector $\hat{\mathbf{k}}$ in terms of the corresponding spherical coordinates, i.e., elevation and azimuth angles $(\theta_r, \phi_r) \in \mathcal{S}_+$.

REFERENCES

- [1] T. L. Marzetta, "Spatially-Stationary Propagating Random Field Model for Massive MIMO Small-Scale Fading," in *2018 IEEE Int. Symposium Inf. Theory (ISIT)*, June 2018, pp. 391–395.
- [2] A. Pizzo, T. L. Marzetta, and L. Sanguinetti, "Holographic MIMO Communications Under Spatially-Stationary Scattering," 2020. [Online]. Available: <https://arxiv.org/abs/2012.07389>
- [3] T. L. Marzetta, "Book Review: Wave Theory of Information," *IEEE Information Theory Society Newsletter*, pp. 5–6, 2019.
- [4] J. C. Maxwell, "A Dynamical Theory of the Electromagnetic Field," *Philosophical Trans. of the Royal Society of London*, vol. 155, pp. 459–512, 1865.
- [5] C. E. Shannon, "The mathematical theory of communication," *Bell System Technical Journal*, vol. 27, no. 3, pp. 379–423, 1948.
- [6] M. Franceschetti, *Wave Theory of Information*. Cambridge University Press, 2017.
- [7] M. D. Migliore, "On Electromagnetics and Information Theory," *IEEE Trans. on Antennas and Propagation*, vol. 56, no. 10, pp. 3188–3200, 2008.
- [8] W. C. Chew, *Waves and Fields in Inhomogenous Media*. Wiley-IEEE Press, 1995.
- [9] A. M. Sayeed, "Deconstructing Multiantenna Fading Channels," *IEEE Trans. Signal Process.*, vol. 50, no. 10, pp. 2563–2579, 2002.
- [10] V. V. Veeravalli, Yingbin Liang, and A. M. Sayeed, "Correlated MIMO Wireless Channels: Capacity, Optimal Signaling, and Asymptotics," *IEEE Trans. Inf. Theory*, vol. 51, no. 6, pp. 2058–2072, 2005.
- [11] A. S. Y. Poon, R. W. Brodersen, and D. N. C. Tse, "Degrees of Freedom in Multiple-antenna Channels: a Signal Space Approach," *IEEE Trans. Inf. Theory*, vol. 51, no. 2, pp. 523–536, Feb 2005.
- [12] A. S. Y. Poon, D. N. C. Tse, and R. W. Brodersen, "Impact of Scattering on the Capacity, Diversity, and Propagation Range of Multiple-Antenna Channels," *IEEE Trans. Inf. Theory*, vol. 52, no. 3, March 2006.
- [13] T. D. Abhayapala, T. S. Pollock, and R. A. Kennedy, "Spatial Decomposition of MIMO Wireless Channels," in *Seventh International Symposium Signal Process. and Its Applications, 2003. Proceedings.*, vol. 1, 2003, pp. 309–312.
- [14] T. S. Pollock, T. D. Abhayapala, and R. A. Kennedy, "Spatial Limits to MIMO Capacity in General Scattering Environments," in *7th International symposium on DSP Communication Systems (DSPCS03)*, vol. 1, 2003, pp. 49–54.
- [15] A. Pizzo, T. L. Marzetta, and L. Sanguinetti, "Spatially-Stationary Model for Holographic MIMO Small-Scale Fading," *IEEE Journal on Selected Areas in Communications*, vol. 38, no. 9, pp. 1964–1979, 2020.
- [16] D. Dardari and N. Decarli, "Holographic Communication using Intelligent Surfaces," 2020. [Online]. Available: <https://arxiv.org/abs/2012.01315>
- [17] S. Hu, F. Rusek, and O. Edfors, "Beyond Massive MIMO: The Potential of Data Transmission With Large Intelligent Surfaces," *IEEE Trans. Signal Process.*, vol. 66, no. 10, pp. 2746–2758, 2018.
- [18] Q. Wu and R. Zhang, "Intelligent Reflecting Surface Enhanced Wireless Network: Joint Active and Passive Beamforming Design," in *2018 IEEE Global Communications Conference (GLOBECOM)*, 2018, pp. 1–6.
- [19] E. Basar, M. Di Renzo, J. De Rosny, M. Debbah, M. S. Alouini, and R. Zhang, "Wireless Communications Through Reconfigurable Intelligent Surfaces," *IEEE Access*, vol. 7, pp. 116 753–116 773, 2019.
- [20] M. Di Renzo, A. Zappone, M. Debbah, M. S. Alouini, C. Yuen, J. de Rosny, and S. Tretyakov, "Smart Radio Environments Empowered by Reconfigurable Intelligent Surfaces: How It Works, State of Research, and The Road Ahead," *IEEE Journal on Selected Areas in Communications*, vol. 38, no. 11, pp. 2450–2525, 2020.

- [21] E. Björnson, H. Wymeersch, B. Matthiesen, P. Popovski, L. Sanguinetti, and E. de Carvalho, "Reconfigurable Intelligent Surfaces: A Signal Processing Perspective With Wireless Applications," 2021. [Online]. Available: <https://arxiv.org/abs/2102.00742>
- [22] A. Amiri, M. Angelichinoski, E. de Carvalho, and R. W. Heath, "Extremely Large Aperture Massive MIMO: Low Complexity Receiver Architectures," in *2018 IEEE Globecom Workshops (GC Wkshps)*, 2018, pp. 1–6.
- [23] Y. Xing, T. S. Rappaport, and A. Ghosh, "Millimeter Wave and sub-THz Indoor Radio Propagation Channel Measurements, Models, and Comparisons in an Office Environment," 2021. [Online]. Available: <https://arxiv.org/abs/2103.00385>
- [24] Y. Xing and T. S. Rappaport, "Terahertz Wireless Communications: Research Issues and Challenges for Active and Passive Systems in Space and on the Ground above 100 GHz," 2021. [Online]. Available: <https://arxiv.org/abs/2103.00604>
- [25] D. A. B. Miller, "Communicating with waves between volumes: evaluating orthogonal spatial channels and limits on coupling strengths," *Appl. Opt.*, vol. 39, no. 11, pp. 1681–1699, April 2000.
- [26] L. Hanlen and M. Fu, "Wireless Communication Systems with Spatial Diversity: a Volumetric Model," *IEEE Trans. Wireless Commun.*, vol. 5, no. 1, pp. 133–142, 2006.
- [27] N. Zheludev and Y. Kivshar, "From Metamaterials to Metadevices," *Nature Materials*, vol. 11, no. 1, pp. 917–924, 2012.
- [28] T. L. Marzetta, "BLAST Arrays of Polarimetric Antennas," Nokia Proprietary, ITD-01-41984K, 10 05 2001.
- [29] T. Marzetta, E. Larsson, and T. Hansen, "Massive MIMO and Beyond," in *Information Theoretic Perspectives on 5G Systems and Beyond*. Cambridge: Cambridge University Press, 2020.
- [30] T. B. Hansen and A. D. Yaghjian, *Plane-Wave Theory of Time-Domain Fields*. New York: Wiley-IEEE Press, 1999.
- [31] D. S. Saxon, "Tensor Scattering Matrix for the Electromagnetic Field," *Phys. Rev.*, vol. 100, pp. 1771–1775, Dec 1955.
- [32] E. Gerjuoy and D. S. Saxon, "Variational Principles for the Acoustic Field," *Phys. Rev.*, vol. 94, pp. 1445–1458, Jun 1954.
- [33] M. Nieto-Vesperinas and E. Wolf, "Generalized Stokes reciprocity relations for scattering from dielectric objects of arbitrary shape," *Journal of The Optical Society of America A-optics Image Science and Vision*, vol. 3, pp. 2038–2046, 1986.
- [34] M. Franceschetti, "On Landau's Eigenvalue Theorem and Information Cut-Sets," *IEEE Trans. Inf. Theory*, vol. 61, no. 9, pp. 5042–5051, 2015.
- [35] A. Sommerfeld, *Partial Differential Equations in Physics*. Academic Press, 1949.
- [36] P. Bello, "Characterization of Randomly Time-Variant Linear Channels," *IEEE Trans. Commun. Systems*, vol. 11, no. 4, pp. 360–393, 1963.
- [37] E. Wolf, "A scalar representation of electromagnetic fields: II," *Proceedings of the Physical Society*, vol. 74, no. 3, pp. 269–280, sep 1959.
- [38] G. C. Sherman, "Diffracted Wave Fields Expressible by Plane-Wave Expansions Containing only Homogeneous Waves," *J. Opt. Soc. Am.*, vol. 59, no. 6, pp. 697–711, Jun 1969.
- [39] A. J. Devaney and E. Wolf, "Multipole Expansions and Plane Wave Representations of the Electromagnetic Field," *Journal of Mathematical Physics*, vol. 15, no. 2, pp. 234–244, 1974.
- [40] R. H. Stolt, "Migration by Fourier transform," *Geophysics*, vol. 43, no. 1, pp. 23–48, 1978.
- [41] G. Durisi, U. G. Schuster, H. Bölcskei, and S. Shamai, "Noncoherent Capacity of Underspread Fading Channels," *IEEE Trans. Inf. Theory*, vol. 56, no. 1, pp. 367–395, 2010.
- [42] A. L. Moustakas, H. U. Baranger, L. Balents, A. M. Sengupta, and S. H. Simon, "Communication through a diffusive medium: Coherence and capacity," *Science*, vol. 287, no. 5451, 2000.
- [43] H. L. Van Trees, *Detection Estimation and Modulation Theory, Part I*. Wiley, 1968.
- [44] W. Nam, D. Bai, J. Lee, and I. Kang, "On the Capacity Limit of Wireless Channels Under Colored Scattering," *IEEE Trans. Inf. Theory*, vol. 60, no. 6, pp. 3529–3543, 2014.
- [45] C. E. Shannon, "Communication in the Presence of Noise," *Proceedings of the IRE*, vol. 37, no. 1, pp. 10–21, 1949.

- [46] A. Pizzo, T. L. Marzetta, and L. Sanguinetti, "Degrees of Freedom of Holographic MIMO Channels," in *2020 IEEE 21st Int. Workshop Signal Process. Adv. Wireless Commun. (SPAWC)*, 2020, pp. 1–5.
- [47] D. A. B. Miller, "Waves, Modes, Communications, and Optics: a Tutorial," *Adv. Opt. Photon.*, vol. 11, no. 3, pp. 679–825, Sep 2019.
- [48] A. Paulraj, R. Nabar, and D. Gore, *Introduction to Space-Time Wireless Communications*. Cambridge, UK: Cambridge University Press, 2003.
- [49] A. Saleh and R. Valenzuela, "A Statistical Model for Indoor Multipath Propagation," *IEEE Journal on Selected Areas in Communications*, pp. 128–137, 1987.
- [50] R. Heddergott and P. Truffer, "Statistical Characteristics of Indoor Radio Propagation in NLOS Scenarios," Communication Technology Laboratory Swiss Federal Institute of Technology Zurich, Valencia, Spain, Tech. Rep. COST 259 TD (00) 024, 2000.
- [51] M. Toeltsch, J. Laurila, K. Kalliola, A. F. Molisch, P. Vainikainen, and E. Bonek, "Statistical Characterization of Urban Spatial Radio Channels," *IEEE Journal on Selected Areas in Communications*, vol. 20, no. 3, pp. 539–549, 2002.
- [52] Da-Shan Shiu, G. J. Foschini, M. J. Gans, and J. M. Kahn, "Fading Correlation and its Effect on the Capacity of Multielement Antenna Systems," *IEEE Trans. Commun.*, vol. 48, no. 3, pp. 502–513, 2000.
- [53] K. V. Mardia and P. E. Jupp, *Directional Statistics*. New York: John Wiley & Sons, Inc, 2000.
- [54] J. T. Kent, "The Fisher-Bingham Distribution on the Sphere," *Journal of the Royal Statistical Society*, vol. 44, no. 1, pp. 71–80, 1982.
- [55] K. V. Mardia, "Statistics of Directional Data," *Journal of the Royal Statistical Society*, vol. 37, no. 3, pp. 349–393, 1975.
- [56] T. Zwick, C. Fischer, and W. Wiesbeck, "A Stochastic Multipath Channel Model Including Path Directions for Indoor Environments," *IEEE Journal on Selected Areas in Communications*, vol. 20, no. 6, pp. 1178–1192, 2002.
- [57] E. Telatar, "Capacity of Multi-antenna Gaussian Channels," *European Trans. on Telecommunications*, vol. 10, no. 6, pp. 585–595, 1999.
- [58] T. L. Marzetta, "Fundamental Limitations on the Capacity of Wireless Links that use Polarimetric Antenna Arrays," in *Proceedings IEEE International Symposium Inf. Theory*, 2002, pp. 51–.
- [59] M. Franceschetti and K. Chakraborty, "Space-time Duality in Multiple Antenna Channels," *IEEE Trans. Wireless Commun.*, vol. 8, no. 4, pp. 1733–1743, 2009.
- [60] E. Biglieri, J. Proakis, and S. Shamai, "Fading Channels: Information-theoretic and Communications Aspects," *IEEE Trans. Inf. Theory*, vol. 44, no. 6, pp. 2619–2692, 1998.